Received: 20 August 2020 | Revised: 30 June 2021 | Accepted: 31 July 2021

DOI: 10.1002/joc.7374

RESEARCH ARTICLE

International Journal of Climatology RMetS

ENSO and PDO related interannual variability in the north and east-central part of the Bolivian Altiplano in South America

Katherine Rojas-Murillo[1,2] | **Anthony R. Lupo**[1] | **Magali Garcia**[2] | **Jere Gilles**[3] | **Alex Korner**[1] | **Marco A. Rivera**[2]

[1]Atmospheric Science Program, School of Natural Resources, University of Missouri, Columbia, Missouri, USA

[2]Faculty of Engineering, Higher University of San Andres, La Paz, Bolivia

[3]Rural Sociology Program, Division of Applied Social Sciences, University of Missouri, Columbia, Missouri, USA

Correspondence
Katherine Rojas-Murillo, Atmospheric Science Program, School of Natural Resources, University of Missouri, Columbia, MO, USA.
Email: katherinerm1313@gmail.com

Abstract

Previous studies in this region focused on interannual and interdecadal precipitation variability during Dec–Feb (summer), relating the El Niño (EN) phase to droughts. Many studies examine this variability over different parts of the Altiplano, and mountainous terrain is well-known for producing complex climate signals as well as variability over relatively small regions. Studies that have examined climate variability over the Altiplano suggest that the El Nino Southern Oscillation (ENSO) influence is complex. The monthly precipitation, maximum and minimum temperature from 1979 to 2017 are used to examine how ENSO and PDO (Pacific decadal oscillation) influence climate conditions. Power spectra analysis determined the periodicities, and analysis of variance was applied to standardized anomalies of the three variables to evaluate PDO and ENSO as variance factors. Frequency distributions were calculated by PDO and ENSO phases, and the differences were tested using the Chi-square test. Our results suggest a PDO and ENSO influence, displaying more dry anomalies during DJF for EN/PDO(+), in agreement with a northward position of the Bolivian high. More wet anomalies during SON (Sep–Oct–Nov) in Neutral (NEU)/PDO(+) due to an upper-level weak westerly flow during PDO(+). For maximum temperature, a reduction in cold anomalies during EN/PDO(−) was observed along with greater warm anomalies in JJA (Jun–Jul–Aug), SON and MAM (Mar–Apr–May). Similar results were observed for NEU phase, due to a greater occurrence of high pressures centres over the region during the PDO (−). Minimum temperature results displayed more variation within stations and a less clear response to ENSO compared to PDO. The research found a clear influence of PDO in the regional climatology associated with the influence of the upper-level jet stream using the NCEP-NCAR composites. This provided a better understanding of these two phenomena, which would allow the

production of seasonal forecasts based on ENSO and PDO using both surface and upper-level information.

KEYWORDS

Bolivian Altiplano, ENSO, interannual variability, PDO, power spectra, precipitation, surface temperature

1 | INTRODUCTION

The Bolivian Altiplano is a complex region located in the central Andes Mountains. At around 3,600 m.a.s.l (~600 hPa), this plateau is surrounded by the western (Cordillera Real) and eastern (Cordillera Oriental) mountains. Weather forecasting in this region is a challenge due to the strong influence of the upper-level circulation, local topography and sea surface temperature oscillations over the Pacific and the Atlantic oceans. Despite these characteristics, agriculture is the main activity in the region and suffers the consequences of the climate variability at interannual and decadal scales, precipitation being the most variable element.

Precipitation in the Bolivian Altiplano is the main source of water for agricultural activities. However, 80% of precipitation is concentrated from December to March, January being the wettest month, and annual precipitation ranges from 250 to 750 mm (Andrade *et al*., 2018). The wet season is characterized by an upper-level anticyclone known as the Bolivian high (BH) which is observed usually at 200-hPa level using the vector wind and the negative values of velocity potential at 200-hPa show divergence over Bolivia in Dec–Jan–Feb (DJF) (Krishnamurti *et al*., 2013; Segura *et al*., 2020). Thus, the Bolivian Altiplano region has a distinct seasonal cycle, which is called the dry and wet season in the tropical Andes. The dry season is produced by the enhancement of the subtropical jet stream, this westerly flow inhibits the easterly moisture transport. During the wet season, the subtropical jet stream returns to its southern position and the ITCZ enters the continent along with the establishment of the BH, allowing the equatorial easterly flow prevailing in the area (Garreaud *et al*., 2003). Additionally, the onset of the low-level jet (LLJ) season (e.g., Wang and Fu, 2004) allows for the return of moisture convergence and precipitation. Also, Wang and Fu (2004) demonstrated that the South American northerly LLJ is a synoptic feature that is largely responsible for the transport of moisture into the Altiplano region. Segura *et al*. (2020) (their fig. 11) proposes a schematic summarizing the mechanisms controlling precipitation including the LLJ in the Altiplano region. Regarding temperature, Andrade *et al*. (2018) mentioned that maximum temperature ranges from 12 to 16.5°C in their study region, with the maximum values occurring temporally in Sep–Oct–Nov (SON). Minimum temperature varies through the seasons ranging from 0 to 1.5°C in DJF and from −6 to −4.5°C in JJA.

The interannual variability of these meteorological elements, especially precipitation was attributed to the El Nino-Southern Oscillation (ENSO) in the central Andes (e.g., Segura *et al*., 2016; Seiler *et al*., 2013; Cai *et al*., 2020). The ENSO is an oscillation of the atmospheric-ocean interaction that occurs every 3–7 years over the Pacific (Bjerknes, 1969; Gu and Philander, 1995). Certainly, this phenomenon, aside from the global connotation, strongly impacts the Bolivian Altiplano. However, there seems not to be a direct association between the EN and LN phase with dry and wet anomalies over the Altiplano as there are wet EN and dry LN years (Garreaud *et al*., 2003; Perry *et al*., 2017). Different studies have described the ENSO teleconnection in the Altiplano, mainly during the austral summer (Garreaud and Aceituno, 2001; Vuille and Keimig, 2004; Segura *et al*., 2019; Canedo-Rosso *et al*., 2019). Dry anomalies are related to the mid-level and upper-level westerly anomalous flow that inhibits the easterly moisture transport (Garreaud *et al*., 2003; Segura *et al*., 2016, 2019). That relationship was demonstrated by the high correlation between the outgoing longwave radiation and the zonal wind anomalies at 200 hPa over the Altiplano. In spite of the intensified westerly flow during EN years, the relation between canonical EN signal and rainfall anomalies in the Altiplano is weak. This paradox mentioned by Garreaud and Aceituno (2001) could be understood as a highly sensitive response to the position and intensity of the BH which controls the upper-level circulation. A northward position increases westerly flow and the dry event occurrence whereas a southward position increases precipitation (Garreaud *et al*., 2003; Vuille and Keimig, 2004). More recently, Segura *et al*. (2019) showed that meridional temperature gradient could also explain the precipitation variability as a strong meridional temperature gradient is present at 400 hPa between 16 and 20°S during extreme dry events over the Altiplano. Then, a comprehensive review article by Cai *et al*. (2020) examines the impact of ENSO across South America including

an analysis of the impact of central Pacific ENSO related SST anomalies and their associated synoptic and large-scale flow regimes as compared to eastern Pacific ENSO related SSTs.

Additionally, spatial rainfall variability over the Altiplano plays an important role, as previous studies identified two main domains of common variance in this region, those divide the Altiplano in a southwest part that highly correlates with the upper-level zonal winds anomalies (200 hPa) and the northeast Altiplano, which was not completely described due to the lack of information (fig. 6 in Vuille *et al*., 2000; Vuille *et al*., 2000; Vuille and Keimig, 2004). More recent studies, for example, Segura *et al*. (2016), focused on the northern Altiplano or Lake Titicaca region. Regarding temperature, aside from that northeast portion, the rest of the central part of the Bolivian Altiplano (16–19°S/70°W–66°W) showed a less significant ENSO influence. As such, the southwest domain was associated with a temperature increase after 1970 (Vuille and Keimig, 2004). These previous studies have faced the lack of weather information available at that time and the uncertainty related to the spatial variability, especially over the part of the Altiplano that this study is focused on. Moreover, temperature was studied as a mean value omitting the dynamics of maximum and minimum temperature.

More recently, the decadal and interdecadal (e.g., Cai *et al*., 2020; Segura *et al*., 2016, 2020) signal has also been identified in studies of climate variability in South America, especially that associated with the Pacific decadal oscillation (PDO). This oscillation is considered an ENSO-like phenomenon and its interaction with ENSO was studied previously by many authors (Andreoli and Kayano, 2005; Garreaud *et al*., 2009; Kayano and Andreoli, 2009; da Silva *et al*., 2011). These studies were mainly focused on ENSO-related DJF (austral summer) precipitation anomalies and upper-level circulation differences relate to PDO. Andreoli and Kayano (2005) analysed ENSO-related composites of 200-hPa velocity potential, 200-hPa stream function and 500-hPa vertical velocity along with rainfall series from stations along South America with very few stations in the Bolivian Altiplano. The time-period considered in that study was 1948–1999, this range included one negative PDO (1947–1976) and one positive PDO (1977–1998) following Mantua *et al*. (1997). For the Bolivian Altiplano, their results suggest significant dry anomalies during EN/PDO positive although an upper-level description was not presented. The occurrence of dry anomalies during positive PDO and EN is supported by Seiler *et al*. (2013) for the Andes region of Bolivia (southwestern Altiplano) as well. They studied the period from around 1960–2009. Their results certainly suggest significant differences in rainfall anomalies during EN due to PDO and a more organized pattern identification for EN in positive PDO, meaning that the positive phases of PDO and ENSO favour constructively their interaction whereas a relation between opposite phases of ENSO and PDO produces a destructive interaction (Kayano and Andreoli, 2009).

Additionally, Segura *et al*. (2016, 2020) found significant precipitation variability at 8 years or less and 20 years and that warm central Pacific region SSTs were associated with the occurrence of dry anomalies in the central Andes (northern Bolivian Altiplano). The interplay between ENSO (and central Pacific versus eastern Pacific ENSO) and longer-term variability such as PDO was discussed Birk *et al*. (2010) for central North America. Similar interactions occur for South America as shown or discussed by Wang *et al*. (2012), Stueker (2018) and Cai *et al*. (2020), and the latter two showed the distribution of precipitation over the continent as it relates to circulation changes in response to different ENSO types.

All these preceding studies have established a framework for interannual variability in the Andes Mountains and the South American highlands. Therefore, this study intends to place the association of PDO and ENSO into a local approach over the north and east-central part of the Bolivian Altiplano and identify the significant differences in the circulation conditions due to these phenomena. This includes an examination of the prominent Pacific South American (PSA) teleconnection and blocking. Further, these results could be used in the future to create a seasonal range forecasting guidance analogous to previous research for North America (Lupo *et al*., 2007; Birk *et al*., 2010). This study examines also the seasonal, interannual and interdecadal variability of precipitation, minimum and maximum temperatures. No other study has examined the minimum and maximum temperature variability separately. Sections 2 and 3 describe the study parameters and framework, while Section 4 describes the results here.

2 | DATA

The current analysis used time series of monthly precipitation, mean maximum and mean minimum temperatures that covered 41 years (1976–2017). A total of nine meteorological stations were used (Figure 1), seven of them have the three variables, and two stations just contain precipitation. The database was obtained from the National Weather Service of Bolivia (SENAMHI) web page http://senamhi.gob.bo/index.php/sismet. In the region, the daily data have demonstrated to have different quality issues (Hunziker *et al*., 2017, 2018) which limit use of the data to the monthly scale. In order to

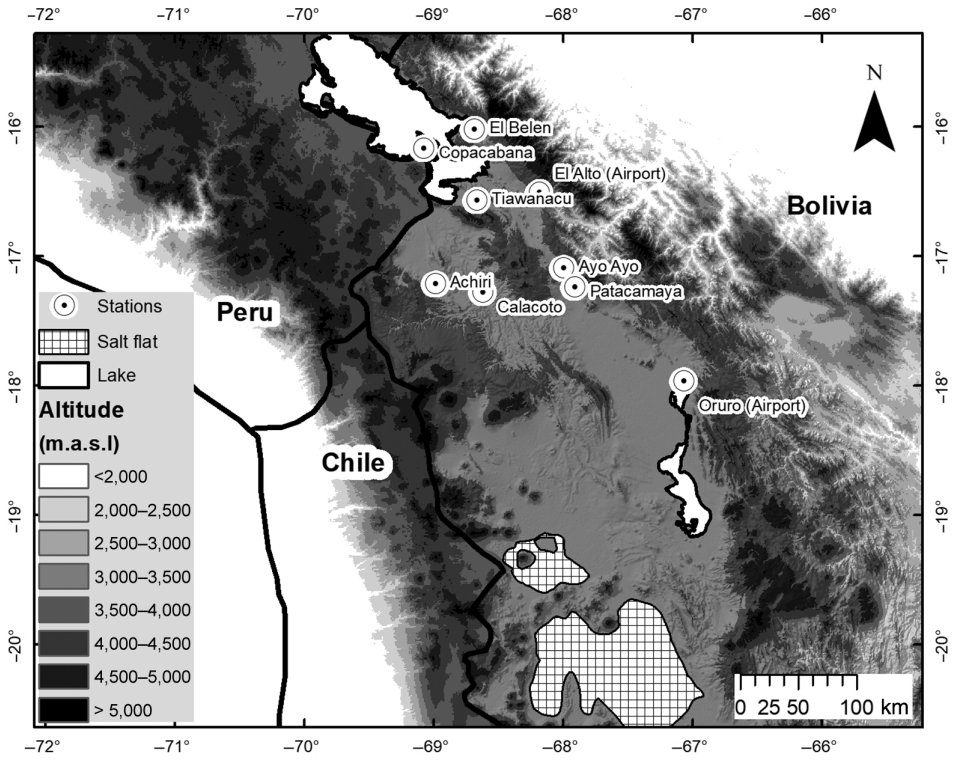

FIGURE 1 Meteorological stations considered in the Bolivian Altiplano

TABLE 1 Coordinates of the meteorological stations used in this study

Station	Tmax and Tmin	Precipitation	Lat. (°)	Lon. (°)	Altitude (m)
Achiri		X	−17.215	−69.001	3,918
El Alto (Airport)	X	X	−16.510	−68.198	4,037
Ayo Ayo	X	X	−17.092	−68.007	3,895
El Belen	X	X	−16.020	−68.699	3,830
Calacoto	X	X	−17.280	−68.635	3,835
Copacabana		X	−16.169	−69.088	3,871
Oruro (Airport)	X	X	−17.966	−67.079	3,719
Patacamaya	X	X	−17.239	−67.922	3,799
Tiawanacu	X	X	−16.568	−68.678	3,868

reduce the data quality issues in this study, the selection of the meteorological stations was based on the following considerations: (a) the quality control flags based on the Data on climate and Extreme weather for the Central AnDEs (DECADE) project, (b) datasets with a maximum of 10% of missing data and (c) time series that extend back unbroken to 1976 if possible. The nine meteorological stations are spread along the north and central part of the Bolivian Altiplano region (Table 1), all these stations coincide with one of the six clusters of precipitation in the Central Andes reported by Hunziker *et al.* (2018) who applied an agglomerate hierarchical clustering to data in Bolivia. In spite of the quality control, Hunziker *et al.* (2018) found data quality issues with the monthly data for minimum temperatures, which is a particular variable that in general is more variable and spatially heterogeneous compared to maximum temperature, and this may impact our results here. As mentioned by WMO (2011), for monthly cumulation the data quality issues could be less significant compared to daily observations, the case of monthly precipitation.

The upper air data were provided through the National Centers for Environmental Prediction/National Center for Atmospheric Research (NCEP/NCAR) re-analyses, archived at the NCAR research facilities in Boulder, CO (e.g., Kalnay *et al.*, 1996; Kistler *et al.*, 2001), which can be used to provide large-scale meteorological data on a 2.5° × 2.5° latitude–longitude grids.

2.1 | Pacific decadal oscillation

The PDO is an ENSO-like interdecadal climate pattern, which has two phases, the positive phase consists of cold anomalies at the western and north-central Pacific along with warm anomalies over east and tropical Pacific, including an anomalously deep Aleutian low. The opposite characteristics occur in the negative phase. The mechanisms that produce PDO are not clear (Mantua and Hare, 2002); some studies have concluded that PDO is a result of combined physical processes such as tropical forcing and the atmosphere–ocean interaction in the North Pacific (Newman *et al*., 2016).

Although the PDO area is more focused on the North Pacific, Folland *et al*. (2002) have indicated that it is similar to the IPO (Interdecadal Pacific Oscillation) which is a Pacific basin-wide pattern. The PDO has multidecadal (50–70 years) and interdecadal intervals (15–20 years; Mantua *et al*., 1997). The time series of this study includes two distinct phases of PDO, the positive phase corresponding to 1977–1998 and the following negative phase from 1999 to 2017, periods defined in previous studies (Bove *et al*., 1998; Lupo *et al*., 2007; Birk *et al*., 2010; Henson *et al*., 2017; Lupo *et al*., 2019). The PDO Index (http://research.jisao.washington.edu/pdo) is not uniformly negative or positive during an entire epoch as described above. However, as demonstrated by published studies (e.g., Kung and Chern, 1995; Tilly *et al*., 2008; Birk *et al*., 2010; Wang *et al*., 2012; Stueker, 2018) and references therein, it is the spatial distribution of the SST anomalies that is associated with atmospheric Flow regimes. In particular, it is the curvature of the SST distribution (e.g., Tilly *et al*., 2008) that will have an impact on the atmospheric height or pressure field.

2.2 | El Nino Southern Oscillation

The ENSO index according to the Japanese meteorological agency (JMA) was used in this study to define the ENSO years. This is provided by the COAPS (Center for Ocean-Atmospheric Prediction Studies) which is a 5-month running mean of spatially averaged sea surface temperatures anomalies over an area (4°S–4°N, 150°W–90°W) in the tropical Pacific. These years are classified as El Nino (La Nina) if the anomalies exceed or are equal to 0.5 C (−0.5 C) for six consecutive months, the values between are known as Neutral years. This index is widely used in different studies (e.g., Lupo *et al*., 2007; Birk *et al*., 2010; Henson *et al*., 2017; and references therein) as it classifies an entire year defined as 1 October to 30 September. For instance, if 1982 is classified as EN, the year is defined as October 1982 to September 1983, which has some similarities with the agriculture cycle in this region that influences the crop yield of the Altiplano region in Bolivia. The JMA ENSO index was chosen over the Southern Oscillation Index, which is relatively noisy (Bove *et al*., 1998) to keep consistency with the background studies mentioned above. The JMA index uses observed SSTs and anomalies obtained using their own ocean data assimilation system and the index is also available through the JMA (https://ds.data.jma.go.jp/tcc/tcc/products/elnino/index.html) Table 2 contains a list of years classified by ENSO phases modified after COAPS (https://www.coaps.fsu.edu/jma).

TABLE 2 Classification of the period of study (1976–2017) based on ENSO index according to JMA and Lupo *et al*. (2008), adapted from COAPS

La Niña (LN)	Neutral (NEU)	El Niño (EN)
1988	1977–1981	1976 (ENs)
1998	1983	1982 (ENs)
1999	1984	1986 (ENw)
2007	1985	1987 (ENw)
2010	1989	1991 (ENw)
	1990	1997 (ENs)
	1992–1996	2002 (ENc)
	2000	2006 (ENc)
	2001	2009 (ENc)
	2003–2005	2014 (ENw)
	2008	2015 (ENs)
	2011–2013	
	2016	

Recent work has shown that the classification of ENSO modes is not uniform and these modes can vary in their intensity as well as the location of the maximum SST anomaly. Some EN are associated with the strongest SST anomaly occurring over the central Pacific (ENSO Modoki) versus the eastern Pacific (Canonical or Classic; e.g., Ashok *et al*., 2007; Takahashi *et al*., 2011; Ren and Jin, 2013; Stueker, 2018). These distinct SST distributions are associated with their own upper air patterns (e.g., North America—Kung and Chern, 1995; Birk *et al*., 2010; South America—Cai *et al*., 2020) and these may influence local climate in a unique way (e.g., Kung and Chern, 1995; Lupo *et al*., 2008; Birk *et al*., 2010; Cai *et al*., 2020). For example, the latter three references demonstrate that the central Pacific EN is associated mainly with a negative (positive) 500 hPa height anomaly over western (eastern) North America and these years are labelled as (ENc). The east Pacific EN is associated with a

strong SST anomaly along Central America (ENs) or a weaker more elongated eastern Pacific SST anomaly (ENw). Both of these EN types produced positive 500 hPa height anomalies over central and northern North America and negative height anomalies upstream and downstream of the central continent and along the southernmost regions. In the southern hemisphere, for example, studies such as O'Kane *et al*. (2017) and Cai *et al*. (2020) and references therein argue that the strength and phase of ENSO are associated with distinct teleconnections as well. In Table 2, we use the classification for EN events inspired by Birk *et al*. (2010). The prevalence of ENc (ENs and ENw) events during the negative (positive) phase of the PDO is consistent with Lupo *et al*. (2008), Stueker (2018) and Cai *et al*. (2020).

3 | METHODS

3.1 | Filtering

The time series were smoothed using a second-order Shapiro filter or a 2-year running mean filter, to extract the low order variability. The 2-year running mean filter could be used to remove the higher frequency noise, seasonal and quasi-biennial oscillations preserving at the same time the dominant oscillations with time scales longer than 2 years (Mokhov *et al*., 2004). This procedure was also simpler to use and implement for examining interannual and interdecadal variability. On the other hand, the Shapiro (1970) filter (Equation 1—where x_i is the variable to be filtered at the i^{th} gridpoint) yields a more robust signal of the lower frequencies compared with the 2 years running mean in power spectra analysis and does not introduce aliasing errors; the modified version was applied several times on the time series (in lieu of using a high order filter) of this study as in Lupo *et al*. (2007) (and references therein) in order to produce a sharper cut off of the higher frequency noise (Shapiro, 1970) and revealing a bi-annual signal, especially for precipitation (see Figure 2a,b). Those filters were applied in other studies of variability such as Birk *et al*. (2010) and Mokhov *et al*. (2004). The resultant filtered time series of the different meteorological stations for the three variables were used in the power spectra analysis.

3.2 | Power spectra analysis

The construction of the power spectra is based on harmonic analysis, which consists of representing the time-series variation as a set of sine and cosine functions. If the dynamical system is sinusoidal and behaves like a regular pendulum, the equation that represents that behaviour can be solved by using empirical orthogonal functions, Fourier series in this case (Birk *et al*., 2010; Lupo *et al*., 2012; Henson *et al*., 2017). Scientific software uses the Fast Fourier Transformation (FFT) instead which provides better and faster algorithms that use the Euler complex exponential rather than sines and cosines. The time series is now a set of Fourier coefficients, amplitudes, which are a function of frequency. The power spectra known as periodogram or Fourier line spectrum consist of squared amplitudes as a function of frequency, showing as the proportion of the time-series variation, the contribution of different oscillations at the harmonic frequency embedded in the time-series (Wilks, 2006). The process was applied to the time series itself and to the filtered time series using the two-year running mean and the Shapiro filter (e.g., Figure 2c,d). The spectral peaks were tested for significance against the white and red noise, which are the theoretical spectral density function of the simple autoregression model (Wilks, 2006; Henson *et al*., 2017). Additionally, the power spectra of the JMA index and climate information were blended using cross-spectral analysis (see Henson *et al*., 2017 and references therein). The resulting covariance spectra will yield the dominant periods shared by the JMA Index (an SST Index) and the climate variables and these were tested against a white noise continuum at $p = .05$.

3.3 | Statistical analysis

After the long-scale oscillations have been identified in the time series, the surface observations response to large-scale variability was analysed. Two statistical analyses of the surface observations were performed to identify the significant differences in climate conditions due to ENSO and PDO. The first one consists of an analysis of variance (ANOVA) of standardized anomalies, also known as normalized anomalies that were calculated by

$$x_i = \frac{186 * x_i + 56 * (x_{i-1} + x_{i+1}) - 28 * (x_{i-2} + x_{i+2}) + 8 * (x_{i-3} + x_{i+3}) - (x_{i-4} + x_{i+4})}{256} \quad (1)$$

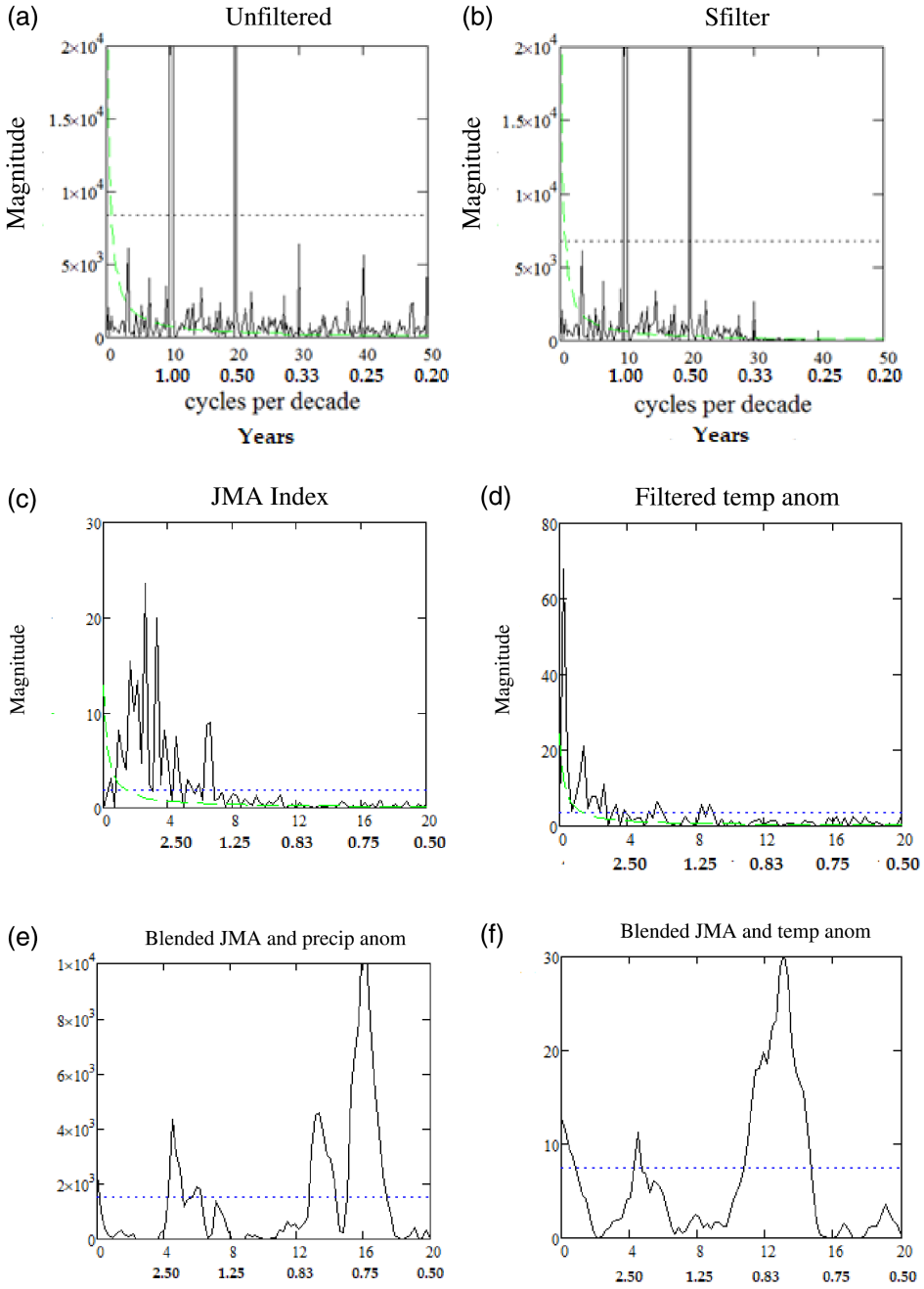

FIGURE 2 Power spectra of (a) unfiltered and (b) Shapiro filtered time series of monthly precipitation, and, (c) JMA Index, (d) 24-month running mean temperature and (e) and (f) blended JMA and precipitation and temperature, respectively for the station 'Calacoto'. The dotted (dashed) line represents the 95% confidence level against the white (red) noise. The ordinate is spectral power and the abscissa is labelled with cycles per decade (top scale) and years (bottom scale) following Wang *et al.* (2012) [Colour figure can be viewed at wileyonlinelibrary.com]

dividing the anomalies by the climatological standard deviation (IRI, 2019). The complete time series per month was used to determine the mean and the standard deviation. The standardized anomalies show the magnitude of the anomalies due to the removal of dispersion. Then, ANOVA allowed to evaluate simultaneously the effect of two or more variables on a response variable. In this case, the standardized anomalies using ENSO and PDO phases as sources of variation. The main assumption of the ANOVA is normality, which was tested with a normality plot of the residuals (quantiles of the residuals against the normal distribution). Monthly temperature residuals fitted the normal distribution. In the case of the monthly precipitation, a logarithm was applied on the time series to fit the residuals to a normal distribution. The statistical analysis used is similar to Birk *et al.* (2010) and Seiler *et al.* (2013).

In the second part of the statistical analysis, monthly anomalies were classified as warm (cold) with respect to temperature or wet (dry) concerning precipitation, if the value is greater (less) than one positive (negative) standard deviation. Frequency distribution plots were built by separating the years by ENSO and PDO phases, the number of EN, LN and NEU years per PDO phase is

TABLE 3 The number of EN, LA and NEU years in the two PDO phases considered in the study

	PDO(+)	PDO(−)
EN	5	6
LA	2	3
NEU	15	11

shown in Table 3. The differences between distributions were tested using Chi-squared goodness of fit, the EN and LN phases were tested against neutral years and later against each other, to see significant differences among them under the influence of PDO.

4 | RESULTS AND DISCUSSION

The first part of results is showing the power spectra plots, which validate the influence of ENSO and PDO on the three monthly variables. Then, the statistical analysis results are organized by variable having first precipitation, second, maximum temperature and minimum temperature. After the explanation of each variable results, composite analysis of the upper level atmosphere are present to support and explain some of the main findings.

4.1 | Power spectra and correlation

The power spectra plots using the unfiltered or Shapiro filtered time series produced similar results between stations especially for precipitation. Significant peaks in monthly precipitation, maximum and minimum temperatures are in agreement with the strong seasonality and the annual cycle present in this area. Monthly precipitation power spectra for the Calacoto station are displayed in Figure 2a (raw) and Figure 2b (filtered) and show two strongly statistically significant peaks for the annual and semi-annual period (wave number of 10 and 20) along the nine weather stations. These peaks reflect the dry and wet seasons in the study region as described by references in the Introduction An explanation is the onset of the LLJ season (e.g., Wang and Fu, 2004; Segura *et al*., 2020) allows for the return of moisture convergence and precipitation. Similar results were found for the rest of the stations (not shown here).

Most (four) of the stations show statistically significant variability ($p = .05$) at approximately 20 years (0.5 cycles per decade). The blended spectra show this 20-year variability in the Lake Titicaca region as well as Ayo Ayo and Patacamaya. This is consistent with the interdecadal variability found in Segura et al. (2016) for the Northern Bolivia Altiplano and at 15–20 years found in other regions (Mantua and Hare, 2002; Lupo *et al*., 2007). Besides, a study at the East of the Altiplano, within the Bolivian valleys have found longer term periodicities of 28–33 years (Amaya *et al*., 2018). Calacoto (Figure 2e) suggests significant longer-term variability than 20 years as well, however, peaks found when discrete transforms such as those used here will be a function of the length of the dataset. Every station showed significant variability at 2–3 years, the rest of the peaks are significant variations of monthly precipitation from 2–5 years. All of them are confirming the relationship with ENSO (Vuille *et al*., 2000; Garreaud *et al*., 2003; Vuille and Keimig, 2004). The blended spectra would also show that the 2–5-year variability is significant ($p = .05$) at all stations, except for Calacoto (Figure 2e) and Patacamaya which suggest 2–3-year variability. This is consistent with many studies of this region such as Seiler *et al*. (2013), Segura et al. (2016) or Cai *et al*. (2020) and references therein.

In Figure 2c, the power spectrum for the raw JMA Index is shown. This index is constructed as an SST index described in Section 2, and as it is calculated using a running mean, sub-annual frequencies would be somewhat muted. There is significant periodicity identified at the largest wave numbers and in the interannual time-frame. Figure 2d is the power spectrum for the 24-month running mean temperature anomaly at Calacoto station, and Figure 2f is the blended power spectra (covariance) from Figure 2c,d. In Figure 2f, the blended frequencies at 2–3 years and 10 years and longer are significant at $p = .05$ confidence level. Decadal-scale variability in this region would be consistent with the findings of Segura et al. (2016) or Cai *et al*. (2020). Similar results can be shown for the other stations for both temperature and precipitation and will be discussed below.

The 24-month running mean of the maximum temperature power spectra are represented in Figure 3, significant variability ($p = .05$) at approximately 20 years and approximately 3–7 years are found for all the stations. Significant variability at 4 years is found for five of the seven stations. These periodicities are also coincident with the ENSO phase. The blended spectra were all similar to Figure 2f, as significant variability was found for five of the seven stations at 20 years, and all of them at 2–3 years. Regarding the minimum temperature, the power spectra plots look similar to those in Figure 3 (not shown) but display minor differences among stations. Periodicity at approximately 20 years is significant for all the stations, but variability at 10 years was significant for six of the seven stations. The periodicities of about 7 and 4 years were statistically significant for four (Patacamaya, Tiawanacu, El Alto, El Belen) and six (all but Tiawanacu) of the seven stations, respectively.

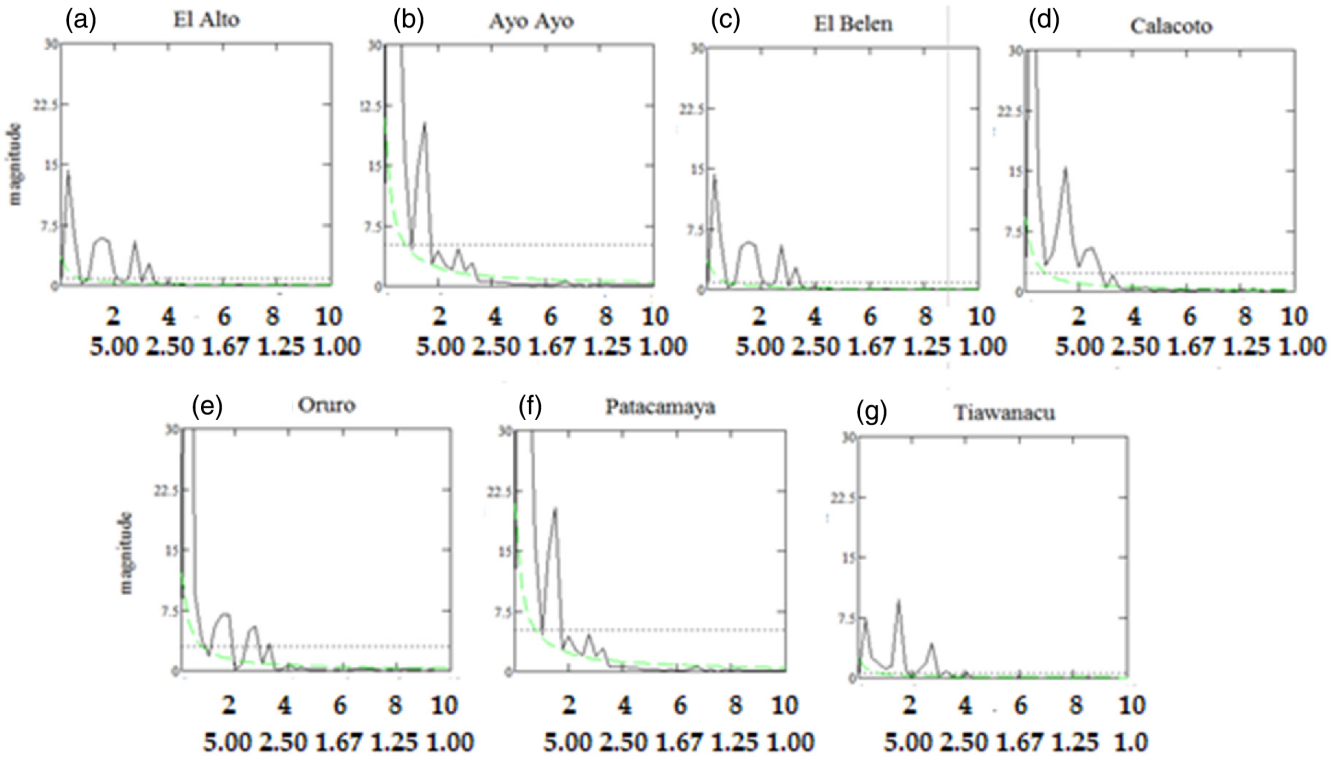

FIGURE 3 Power spectra of the 24-month running mean filtered times series of monthly maximum temperatures for all the meteorological stations in the study area. The ordinate and abscissa are labelled as in Figure 2

In summary, interannual (2–7 years) and interdecadal (20 years) variability likely associated with ENSO and PDO in general are present in all the variables. The blended spectra (temperature or precipitation with the JMA Index) suggest results that were similar to studies such as Segura *et al.* (2016) or Cai *et al.* (2020). Finally, the minimum temperature displayed significant variations every 10 and 4 years in most of the stations. The seasonal results will be discussed below.

Additionally, the correlation between the JMA time series and the maximum temperature anomaly time series from each station ranged from 0.17 (Ayoayo) to 0.30 (Calacoto), and these are all significant at $p = .01$ or higher. The minimum temperature time series showed more complex behaviour when correlating to the JMA Index. Three stations correlated positively at $p = .05$ (El Alto—.11; Patacamaya—.09) or $p = .10$ (Oruro—.05), while three correlated negatively at $p = .05$ (Calacoto−−.08) or $p = .10$ (Tiawanacu and Ayo Ayo). Only El Belen showed no significant correlation with the JMA Index for the minimum temperature. For precipitation, the correlations were not as strong and were all negative (dry anomalies correlating with positive JMA SSTs). Correlations significant at the $p = .01$ were identified for the Achiri station, $p = .05$ (−.08 to −.11) at three of the stations (Calacoto, Copacabana and Oruro), and two (Ayoayo and El Belen) correlated at only $p = .10$ (−.05 to −.08). In order to eliminate the possibility of interannual variability associated with the Quasi-Biennial Oscillation (QBO), correlations with the QBO index (https://www.cpc.ncep.noaa.gov/products/CDB/editors.shtml) were between −.04 and .03 for each station.

4.2 | Monthly and seasonal precipitation results

To examine the effect of PDO and ENSO phases on precipitation, the ANOVA was applied using the standardized anomalies. Figure 4 shows the percentage of months classified as normal (within one standard deviation) and above or below normal as classified by PDO, ENSO. Then, Table A1 shows the seasonal means classified by ENSO and PDO phase. From a visual examination (Figure 4), more drier anomalies are observed during EN for the positive phase of PDO (Andreoli and Kayano, 2005) compared to the negative phase of PDO. Wet anomalies are present along all seasons for both PDO's during EN phase (Figure 4). Meanwhile, LN provided only 1 year for the positive PDO phase, thus, those results will not be considered henceforth, as they are not reliable. But NEU years (Figure 4) have shown interesting differences between

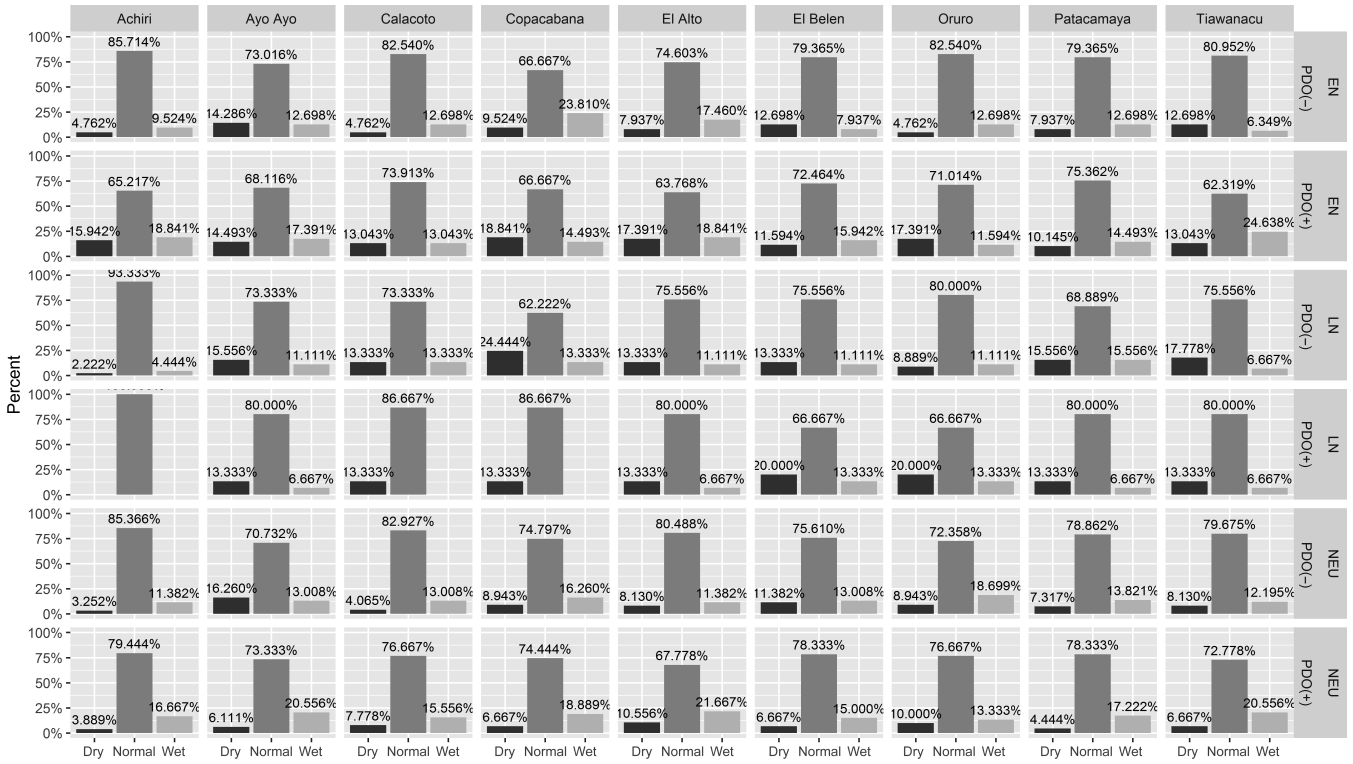

FIGURE 4 Frequency distribution of dry(black)/normal(grey)/wet(light grey) months classified by PDO and ENSO phases for every station, considering all the months

PDO phases as there are more and greater wet anomalies during SON and MAM in the PDO (+) compared to PDO (−), and this result is inferred also from Table A1. This table also demonstrates that spring and fall precipitation decreased at six of these stations and were otherwise similar at the other three stations. During DJF (Table A1), five of the stations showed there was more precipitation during DJF in PDO (−) versus PDO (+), but decreases were noted at three stations. However, none of these results were statistically significant. Table A1 also demonstrates that generally for most stations, EN or NEU years are wetter across all seasons, however, only a few of these seasonal differences were significant when comparing to the overall seasonal station mean (as in Seiler *et al.*, 2013). More differences would be significant if sample means were compared instead. Finally, it is observed that differences between EN and NEU phase vary as PDO change but not homogeneously. While our results here agree with Seiler for EN and LN variability in the summer season, the winter season shows less agreement. For example, our results show that LN winters are generally drier and EN winters generally warmer, while Seiler *et al.* (2013) show a more normal distribution. This is likely due to the difference in the study periods and the use of a different ENSO Index.

The differences identified for all months in the visual examination were statistically analysed with the ANOVA, being the phases of PDO and ENSO the factors that could influence precipitation. A .05 level of significance was considered regarding the *p*-values in the contingency tables; Table 4 indicates with asterisk the presence of significant differences in precipitation due to the factors. These results suggest that the change in PDO phase is associated with significant differences in standardized anomalies of precipitation for five of the nine weather stations, similar results are found for ENSO, not for the same stations though. Tables 4 and A1 as well as Figure 4

TABLE 4 Significant *p*-value at .05 level of significance for the analysis of variance of precipitation standardized anomalies

Stations	PDO	ENSO
Achiri	*	*
El Alto		*
Ayo Ayo	*	
Belen	*	
Calacoto		*
Copacabana		*
Oruro	*	
Patacamaya		
Tiawanacu	*	*

TABLE 5 Monthly precipitation anomalies frequencies (%) comparing EN during PDO (+) and PDO (-).

PDO	ENSO	Station	NORMAL (%)	WET (%)	DRY (%)	
PDO (+)	EN	Achiri	65.2	18.8	15.9	*
PDO (−)	EN		85.7	9.5	4.8	
PDO (+)	EN	El Alto	63.8	18.8	17.4	*
PDO (−)	EN		74.6	17.5	7.9	
PDO (+)	EN	Calacoto	73.9	13.0	13.0	*
PDO (−)	EN		82.5	12.7	4.8	
PDO (+)	EN	Ayo Ayo	68.1	17.4	14.5	NS
PDO (−)	EN		73.0	12.7	14.3	
PDO (+)	EN	El Belen	72.5	15.9	11.6	NS
PDO (−)	EN		79.4	7.9	12.7	
PDO (+)	EN	Oruro	71.0	11.6	17.4	*
PDO (−)	EN		82.5	12.7	4.8	
PDO (+)	EN	Copacabana	66.7	14.5	18.8	*
PDO (−)	EN		66.7	23.8	9.5	
PDO (+)	EN	Patacamaya	75.4	14.5	10.1	NS
PDO (−)	EN		79.4	12.7	7.9	
PDO (+)	EN	Tiawanacu	62.3	24.6	13.0	*
PDO (−)	EN		81.0	6.3	12.7	

Note: The (*) indicates the rejecting of the null hypothesis of the chi-square test a significance level of .05.

will help us to understand not just the influence of these oscillations in the magnitude of the anomalies but also their influence on the percentage of wet, dry and normal months. The first comparison was between PDO (+) and PDO (−) concerning EN, LN and NEU years. The second comparison was made between EN and NEU across each PDO phase. The differences were statistically tested by the chi-squared goodness of fit using a significance level of .05, for this test neutral and PDO (−) years were used as expected observations for the first and second comparison, respectively.

The first comparison is between PDO(+)/EN and PDO(−)/EN and there is a slight difference in the distribution of precipitation for stations except for Achiri, El Alto, Calacoto and Tiawanacu which show significant differences during EN due to PDO phases (Figure 4 and Table 5). During NEU years, there is a significant difference in the monthly distribution due to PDO phases in most of the stations such as Achiri, El Alto, Calacoto, Ayo Ayo and Tiawanacu (Table 6). The second comparison between EN and NEU during each PDO phase (Table 7) gave us mostly non-significant differences for EN and NEU years within PDO (+) and PDO (−) except for Achiri, Ayo Ayo and Copacabana which have significant differences just during PDO (+).There are no significant differences consistently in all the stations for EN and NEU during PDO (−).

The statistical results of the global frequency analysis for this variable suggest that as PDO modulates the ENSO impact there may be other factors that play a role in precipitation variability, such as the North Atlantic Oscillation (NAO) among others (Canedo-Rosso et al., 2021; 2019). The PSA pattern will also play a role in precipitation variability for this region (e.g., O'Kane *et al*., 2017; Cai *et al*., 2020). The former study and references therein suggest the PSA1 and PSA2 are associated with wave number three or four across the Pacific to Argentina. PSA1 (PSA2) would be associated with troughing (ridging) over the study region, and are associated with the four (2 year) ENSO variability. The latter study (Cai *et al*., 2020) associates a stronger PSA pattern with EN, and warmer and wetter conditions over the study region during the spring and drier during the summer. Lupo *et al.* (2019) showed that the proportion of east Pacific blocking accounted for approximately 36% of all Pacific blocking agreeing with Oliveira *et al.* (2014), but that a larger fraction of east Pacific blocking or about 45% occurred during EN (LN) years during PDO(−) (PDO(+)). The statistical analysis of precipitation was made under the assumption of PDO modulates the ENSO impact based on previous studies (Gershunov and Barnett, 1998; Goodrich and Goodrich, 2004; Lupo *et al*., 2008) and techniques applied by Lupo *et al.* (2007), Birk *et al.* (2010) and Henson *et al.* (2017).

TABLE 6 Monthly precipitation anomalies frequencies (%) comparing NEU during PDO (+) and PDO (-)

PDO	ENSO	Station	NORMAL (%)	WET (%)	DRY (%)	
PDO (+)	NEU	Achiri	79.4	16.7	3.9	*
PDO (−)	NEU		85.4	11.3	3.3	
PDO (+)	NEU	El Alto	67.8	21.7	10.6	*
PDO (−)	NEU		80.5	11.4	8.1	
PDO (+)	NEU	Calacoto	76.7	15.6	7.8	*
PDO (−)	NEU		82.9	13.0	4.1	
PDO (+)	NEU	Ayo Ayo	73.3	20.6	6.1	*
PDO (−)	NEU		70.7	13.0	16.3	
PDO (+)	NEU	El Belen	78.3	15.0	6.7	NS
PDO (−)	NEU		75.6	13.0	11.4	
PDO (+)	NEU	Oruro	76.7	13.3	10.0	NS
PDO (−)	NEU		72.4	18.7	8.9	
PDO (+)	NEU	Copacabana	74.4	18.9	6.7	NS
PDO (−)	NEU		74.8	16.3	8.9	
PDO (+)	NEU	Patacamaya	78.3	17.2	4.4	NS
PDO (−)	NEU		78.9	13.8	7.3	
PDO (+)	NEU	Tiawanacu	72.8	20.6	6.7	*
PDO (−)	NEU		79.7	12.2	8.1	

Note: The (*) indicates the rejecting of the null hypothesis of the chi-square test a significance level of .05.

Nonetheless, our results verify the first visual inspection in Table A1 and Figure 4, confirming the dry anomalies during EN overall and EN/PDO (+) in DJF and the wet anomalies during EN overall and EN NEU/PDO (+) in SON, respectively. The first finding is in agreement with many previous studies about interannual variability over the Central Andes and specifically the Altiplano (Vuille *et al*., 2000; Garreaud and Aceituno, 2001; Vuille and Keimig, 2004; Seiler *et al*., 2013; Canedo-Rosso *et al*., 2019). These studies also found that the precipitation variability cannot be fully attributed to ENSO as not all EN years correspond to below-average rainfall especially in the Bolivian Altiplano. The PDO influence on the EN phase was observed at the surface but this is also related to upper-level features such as the BH and its position.

Figure 5 shows the composite 500 hPa height anomalies for EN years during PDO(+) and PDO(−) for winter (JJA), spring (SON) and fall (MAM). For winter (Figure 5a,b) and spring (Figure 5c,d), the pattern closely resembles the PSA pattern suggested by Cai *et al*. (2020) or PSA1 and a PSA1 subset as proposed by O'Kane *et al*. (2017). Further, Cai *et al*. (2020) stated that eastern Pacific EN events produced a stronger PSA signature in the South America Sector, and associated stronger blocking events with these seasons. These results confirm the observations of Cai *et al*. (2020) as the EN 500 hPa height anomalies are stronger during all seasons for PDO(+) (Figure 5a,c,e) versus PDO(−) (Figure 5b,d,f). A positive anomaly southwest of South America flanked by two troughs found here is also similar to that found in Cai *et al*. (2020). Recall Table 2 shows that PDO(+) EN are eastern Pacific events, whereas the PDO(−) EN contained more central Pacific (Modoki) or weak eastern Pacific events. Lupo *et al*. (2019) also find that the blocking events in the east Pacific are stronger and more persistent during eastern Pacific EN years than other years during PDO(+). During PDO(−), however, Lupo *et al*. (2019) blocking in this region during EN years are more numerous and stronger as well than other years. The occurrence of blocking in the southern Pacific Region is comparable to that in the northern Pacific and will relate to the position of the storm tracks.

Figure 6 shows the 200-hPa vector wind composites for EN years during the late summer separating the negative and positive PDO, where a northward position of the BH is observed during PDO(+). This enhances the westerly flow over the Bolivian Altiplano and inhibits the easterly moisture transport (Garreaud and Aceituno, 2001, Segura *et al*., 2016, 2020) whereas a southward position of the BH is observed during PDO(−) (Figure 8b), suggesting enhanced easterly flow. These years are wetter, a result that agrees with Segura *et al*. (2020). Additionally, the scalar wind speed at 200-hPa shows the

TABLE 7 Comparison of the precipitation anomalies frequency distribution (%) between EN and NEU years during PDO (+) and PDO (-)

PDO	ENSO	Station	NORMAL (%)	WET (%)	DRY (%)	
PDO (+)	EN	Achiri	65.2	18.8	15.9	*
	NEU		79.4	16.7	3.9	
PDO (−)	EN		85.7	9.5	4.8	NS
	NEU		85.4	11.3	3.3	
PDO (+)	EN	El Alto	63.8	18.8	17.4	NS
	NEU		67.8	21.7	10.6	
PDO (−)	EN		74.6	17.5	7.9	NS
	NEU		80.5	11.4	8.1	
PDO (+)	EN	Calacoto	73.9	13	13	NS
	NEU		76.7	15.6	7.8	
PDO (−)	EN		82.5	12.7	4.8	NS
	NEU		82.9	13	4.1	
PDO (+)	EN	Ayo Ayo	68.1	17.4	14.5	*
	NEU		73.3	20.6	6.1	
PDO (−)	EN		73	12.7	14.3	NS
	NEU		70.7	13	16.3	
PDO (+)	EN	El Belen	72.5	15.9	11.6	NS
	NEU		78.3	15	6.7	
PDO (−)	EN		79.4	7.9	12.7	NS
	NEU		75.6	13	11.4	
PDO (+)	EN	Oruro	71	11.6	17.4	NS
	NEU		76.7	13.3	10	
PDO (−)	EN		82.5	12.7	4.8	NS
	NEU		72.4	18.7	8.9	
PDO (+)	EN	Copacabana	66.7	14.5	18.8	*
	NEU		74.4	18.9	6.7	
PDO (−)	EN		66.7	23.8	9.5	NS
	NEU		74.8	16.3	8.9	
PDO (+)	EN	Patacamaya	75.4	14.5	10.1	NS
	NEU		78.3	17.2	4.4	
PDO (−)	EN		79.4	12.7	7.9	NS
	NEU		78.9	13.8	7.3	
PDO (+)	EN	Tiawanacu	62.3	24.6	13	NS
	NEU		72.8	20.6	6.7	
PDO (−)	EN		81	6.3	12.7	NS
	NEU		79.7	12.2	8.1	

Note: The (*) indicates the rejecting of the null hypothesis of the chi-square test a significance level of .05.

8 ms^{-1} isotachs across Bolivia in PDO(+) (Figure 6c), the same isotach is centred over Lake Titicaca in PDO (−) (Figure 6d), the presence of tight wind speed contours is evident south of Bolivia during the current PDO phase (Figure 6b,d).

Figure 7 shows the 500 hPa height anomalies for winter, spring and fall over the Pacific and South America during NEU years. Note that, the pattern exhibited generally weaker anomaly centres that were 180° out-of-phase with that of EN years (Figure 5) and those shown in Cai *et al*. (2020). LN years (not shown) were also 180° out of phase with EN years, but the anomalies were just as strong as the ENSO counterparts. The NEU (LN) year anomalies resembled the

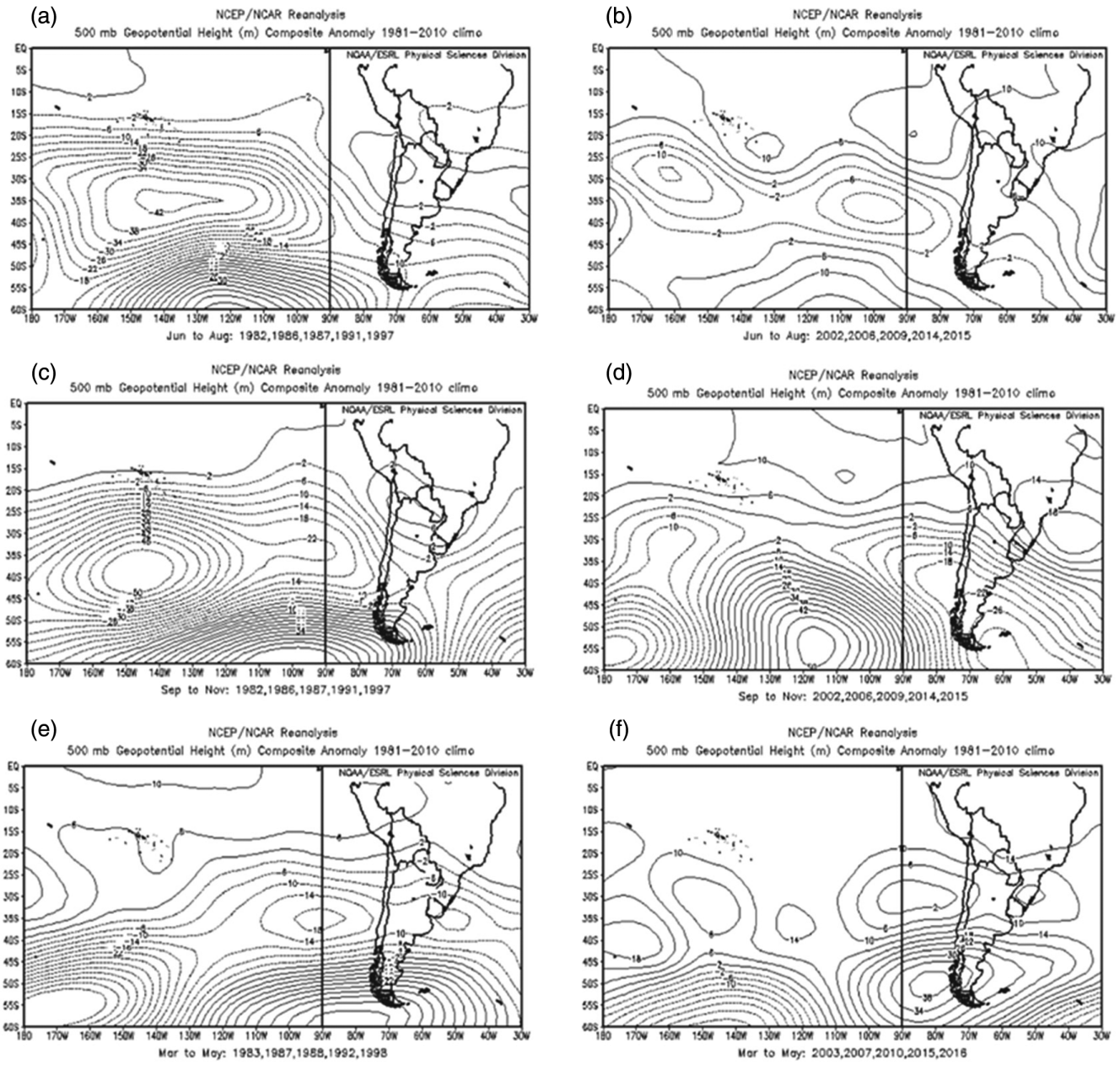

FIGURE 5 Composite of 500-hPa geopotential height anomalies (m) during JJA (a,b), SON (c,d) and MAM (e,f) for PDO (+) (a,c,e) and PDO (−) (b,d,f) in EN phase. The contour interval is 4 m

PSA2 (PSA1) patterns shown by O'Kane *et al*. (2017), and these represented principal components two and three in their study. Our results also showed the PDO influence during NEU years, having more wet anomalies during NEU/PDO (+) and dry anomalies during NEU/PDO (−) for the SON. This trimester is a transition toward the rainy months, the BH is not well established yet over Bolivia and the jet stream advances northward again for SON. These rainfall anomalies are evaluated by looking at the composites of zonal wind anomalies at 200-hPa (Figure 8a,b) and the velocity potential at the 0.201 sigma level (Figure 8c,d), a proxy for divergence in the tropics. From October toward NU/PDO (+) (to the left) and NEU/PDO (−) (to the right). Then, the wet anomalies during NEU/PDO (+) are explained by the anomalous weak westerly flow (Figure 8a) over the Altiplano that would not be able to inhibit moist transport and divergence aloft (Figure 8c) that enhances the upward motion (Segura *et al*., 2016, 2020). Dry anomalies for NEU/PDO (−) are associated with an opposite behaviour and strengthened westerly flow more effective inhibiting the moist transport and the weak divergence would allow downward motion and dry conditions.

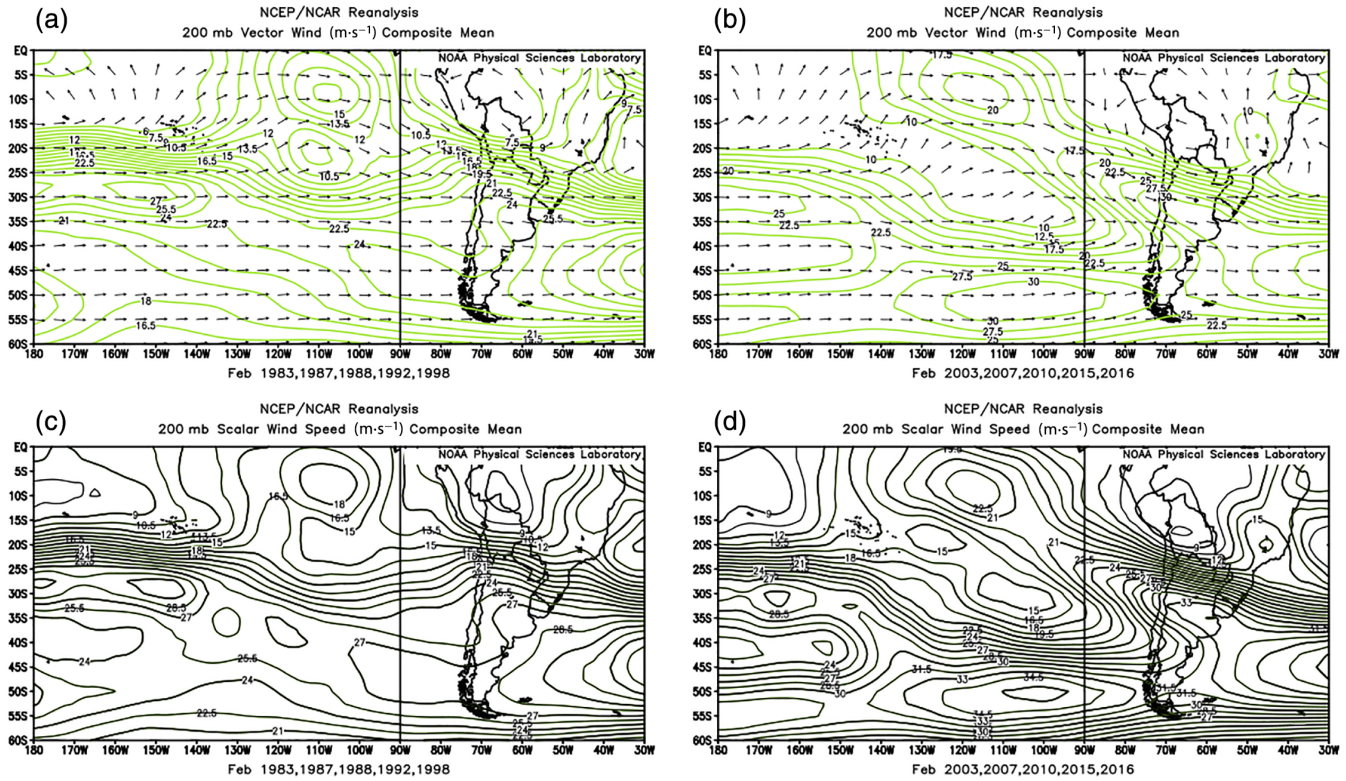

FIGURE 6 The composite mean of 200-hPa vector (arrows) and zonal wind ($m \cdot s^{-1}$) during February after EN for PDO (+) (a) and PDO (−) (b). (c) and (d) as (a) and (b) but for scalar wind ($m \cdot s^{-1}$). The contour interval is 2 $m \cdot s^{-1}$ [Colour figure can be viewed at wileyonlinelibrary.com]

4.3 | Monthly and seasonal maximum and minimum temperature results

As in precipitation, periodicities found through the power spectra analysis for maximum and minimum temperature are in agreement with ENSO and PDO oscillations. Table A2 shows that maximum and minimum temperatures were not universally higher during PDO(−) in spite of the fact that these years are the latter part of the study period. The maximum (minimum) temperature was higher (lower) for Ayo Ayo, Calacoto and El Alto, with the except of summer minimums at El Alto. The result was a stronger diurnal cycle. At Oruro and Patycamaya both maxima and minima were higher, except for spring maxima at the latter station. However, not all the results are statistically significant at even $p = .10$ (Table A2). The results for the other two stations were mixed. Additionally, ENSO variability was stronger in the spring minimum temperature, but in the maximum temperatures for the other seasons. The increase during PDO (−) could also be related to longer term climate trends since our study did not examine temperature information before 1976.

The frequency distribution of warm/cold/normal months of maximum temperature were calculated by station previous classification of the time series by PDO and ENSO phase, which is shown in Figure 9. This figure as in Table A2 also display clear differences due to PDO phase, especially during EN shows more warm and fewer cold months during PDO (−) compared to PDO (+), similar behaviour is observed in NEU phase. In Figure 10 for the minimum temperature, more complex behaviour was noted. For three stations (Oruro, Patacamaya and Tiawanacu) similar behaviour for the minimum temperatures as described for the maxima were noted. But for Ayo Ayo, Calacoto, El Belen there were more cold months and fewer warm months when examining the minimum temperature (Figure 10).

The ANOVA and frequency distribution comparison results are related and it is noticeable the influence of PDO over each ENSO phase, frequency distribution plots by trimester (not shown here) verify the observations in Table A2, Figures 9 and 10. There was a greater number of warm (cold) anomalies during JJA, SON (DJF, MAM and JJA) for EN/PDO (−), and more warm anomalies during DJF for EN/PDO (+) for the maximum temperatures. Even clearer are the differences between EN and NEU phase for the same PDO phase. That is the case of NEU/PDO(+) which does not have more warm anomalies during DJF, on the contrary, more warm anomalies

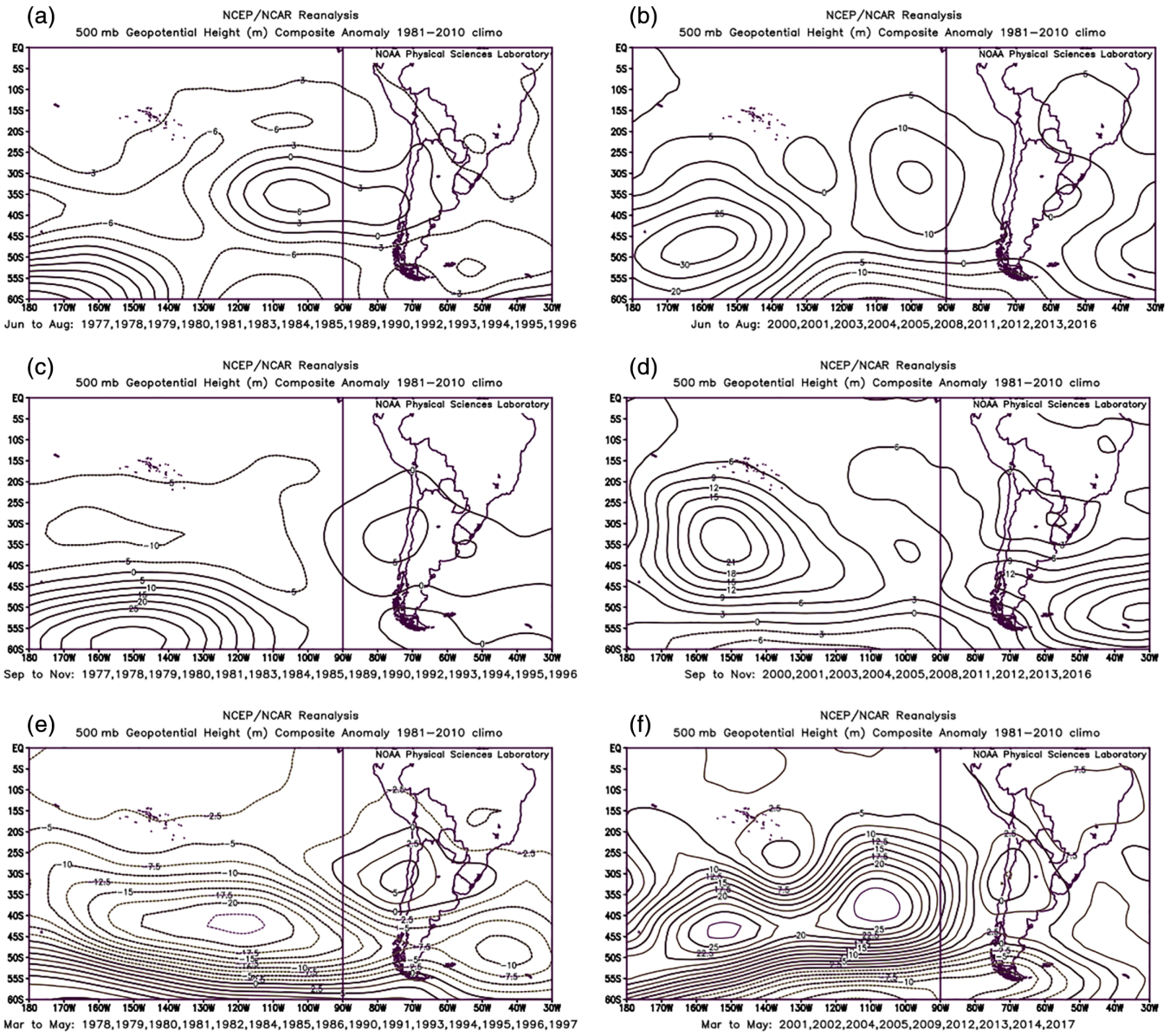

FIGURE 7 As in Figure 5 but for NEU phase [Colour figure can be viewed at wileyonlinelibrary.com]

are present consistently in the four trimesters for NEU/PDO (−) and more cold anomalies for NEU/PDO(+). Therefore, the PDO (−) is characterized by an increment in warm anomalies and a reduction in cold anomalies although this is true for all the trimesters during NEU phase and for some trimesters during EN. Then, maximum temperature has greater percentage of cold anomalies during PDO (+) and greater percentage of warm anomalies for the current PDO phase especially in JJA, SON (DJF, MAM, JJA and SON) for EN (NEU) years.

The results of minimum temperature have shown variations within the stations, probably due to the local effect of the topography and also the local dynamic of water vapour and cloudiness that need to be more studied especially during DJF where the presence of radiative frost could damage the crop production, and also in JJA where the lowest temperatures are crucial for the production of potato sub-products. Nonetheless, it is clear the influence of PDO on ENSO, having fewer cold anomalies in minimum temperatures for the current negative PDO during JJA and DJF for EN years, except for Ayo Ayo and Calacoto that display more cold anomalies for the current PDO phase. Some areas show warm anomalies and others cold ones for the same classification. In the case of Patacamaya, the warm anomalies consistently increase in PDO (−) as the cold anomalies decrease throughout all the trimesters. Finally, recall that Hunziker *et al*. (2018) found data quality issues with the temperature data, especially the minimum temperatures. Our analysis indicated that the minimum temperatures

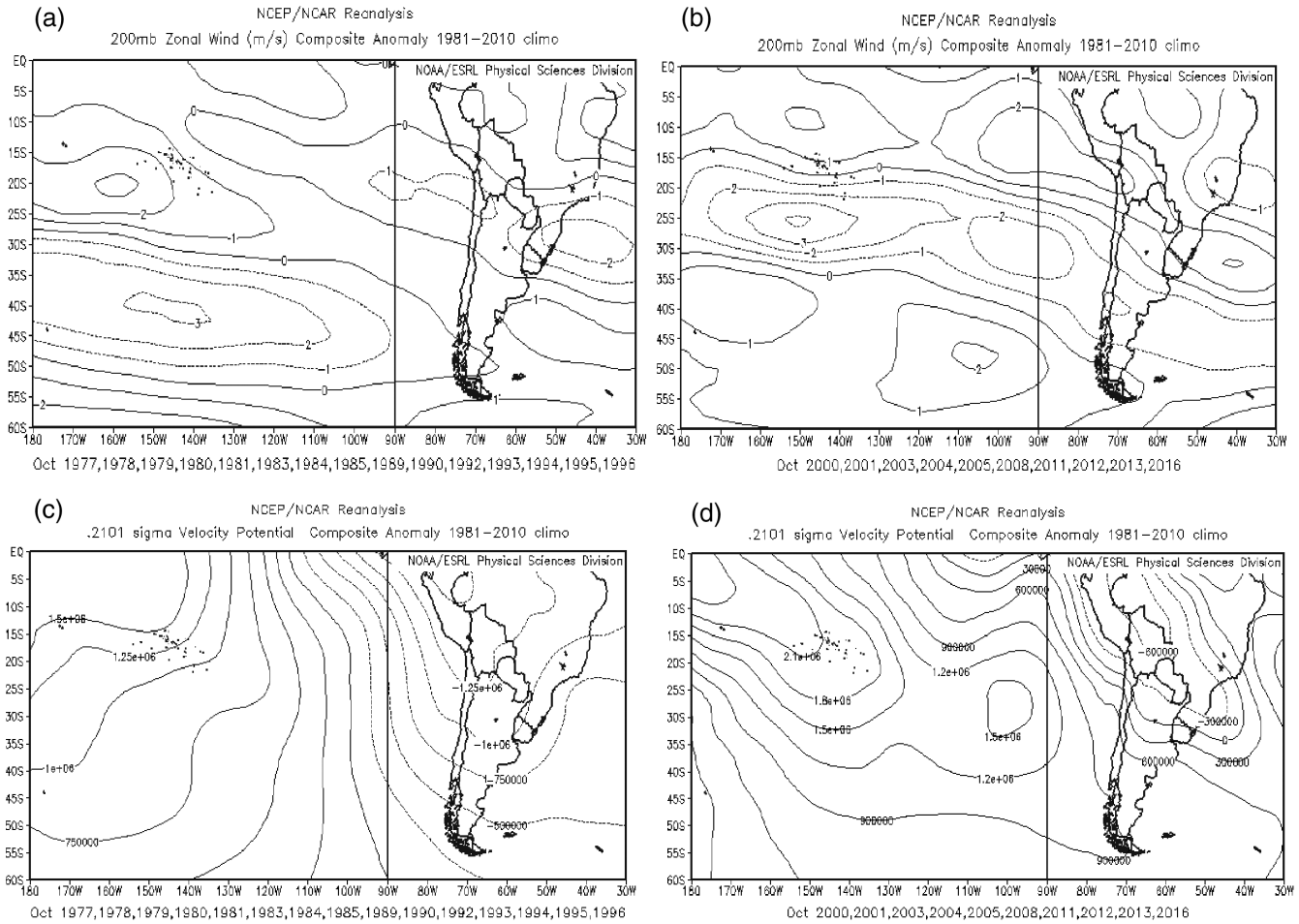

FIGURE 8 The composite mean of 200-hPa zonal wind anomaly ($m \cdot s^{-1}$) during October before NEU for PDO (+) (a) and PDO (−) (b). (c) and (d) as (a) and (b) but for velocity potential ($m^2 \cdot s^{-1}$). The contour interval in (a) and (b) is 1 $m \cdot s^{-1}$, and for (c) and (d) is 2.5×10^5 $m^2 \cdot s^{-1}$

showed less consistency among the stations studied here, than for the maximum temperatures and precipitation. Thus, data quality may explain some of the results as well as local energy balances not fully described by global oscillations. However, the maximum temperature and precipitation results show strong consistency with the analysis of the general circulation.

The main findings were analysed by looking upper-level composites starting with the geopotential height anomalies (Figures 5 and 7) as this variable is related with the changes in temperature, a previous visualization composites of potential temperature and geopotential height anomalies have corroborated that relation (not shown here). In Figure 5a, during JJA, there are heights of 10 gpm above average over the Bolivian Altiplano during PDO (−) compared to PDO (+), similar conditions occur during SON whereas MAM composites show heights of 14 gpm above normal. These anomalies above normal are related to high pressures characterized by clear skies that could allow more incoming solar radiation income that raises the maximum temperature values, but at the same time reduces the cold anomalies in maximum temperature, which would be produced by cloudiness. For those stations that showed a greater diurnal cycle (Table A2), this observation is also consistent with more clear conditions. This is also consistent with the observations of the increased frequency and persistence of blocking during PDO(−), especially during EN years as noted by Lupo *et al.* (2019).

For NEU years, maximum temperature anomalies are similar to in EN years concerning PDO. Figure 7 is showing the 500-hPa geopotential height anomalies for NEU years. JJA composites show slight negative anomalies during PDO (+) (Figure 7a) compared to PDO (−), SON and MAM composites show the same whose heights are 2 gpm below average near the Bolivian Altiplano. Despite the magnitude of the negative anomalies during PDO (+), they are still consistently opposite to PDO (−) which are positive. This explains the warmer anomalies during PDO (−) and the colder anomalies in PDO (+). Those variabilities along with global warming put pressure on small-scale agriculture, which is the main activity in the region.

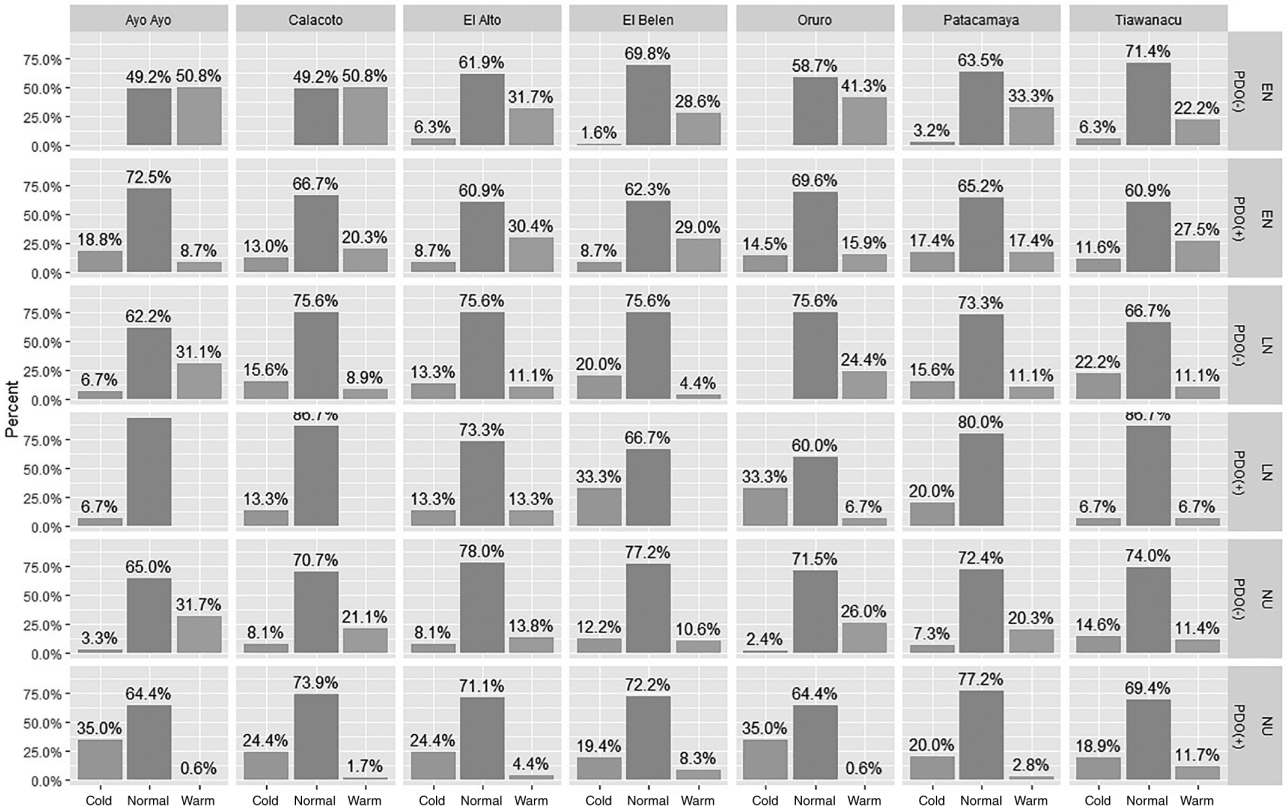

FIGURE 9 Frequency distribution of warm/cold/normal of monthly maximum temperature classified by PDO and ENSO phases for every station, considering all the months

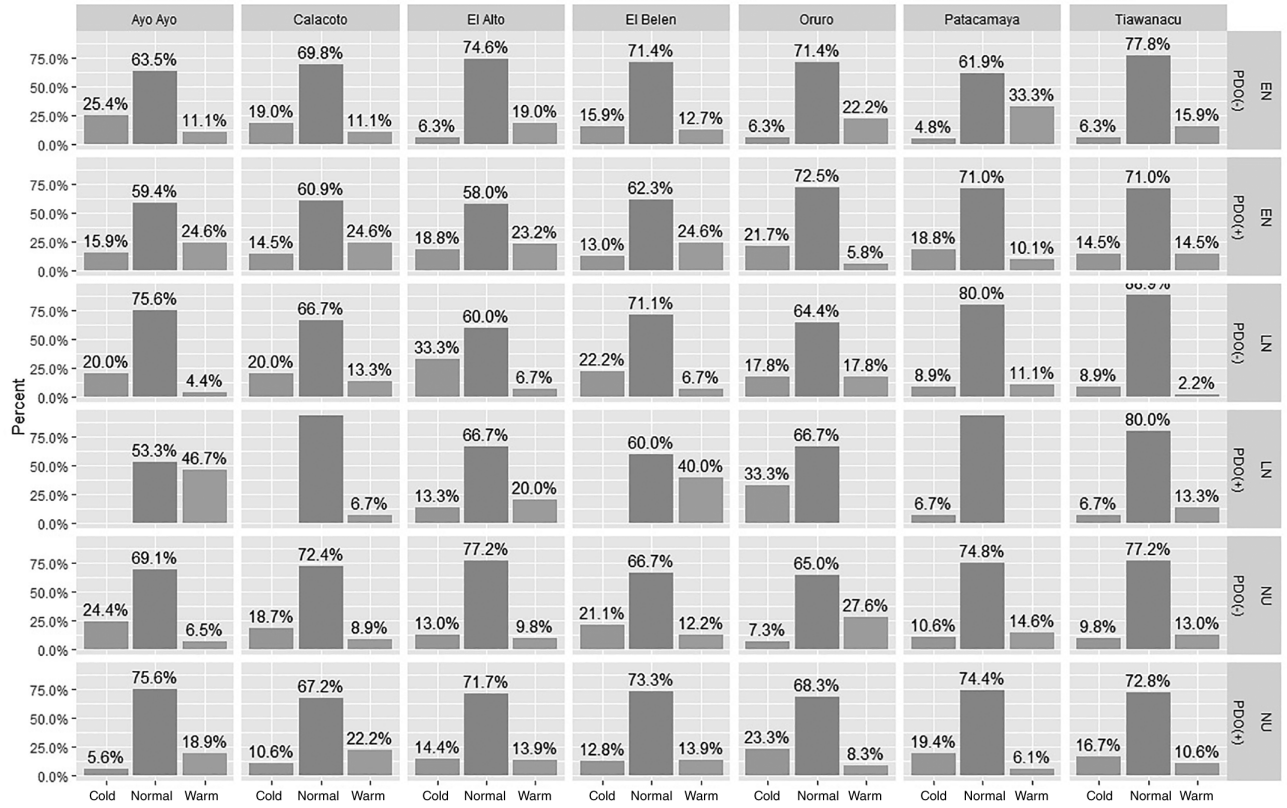

FIGURE 10 As in Figure 9, except for the monthly minimum temperature

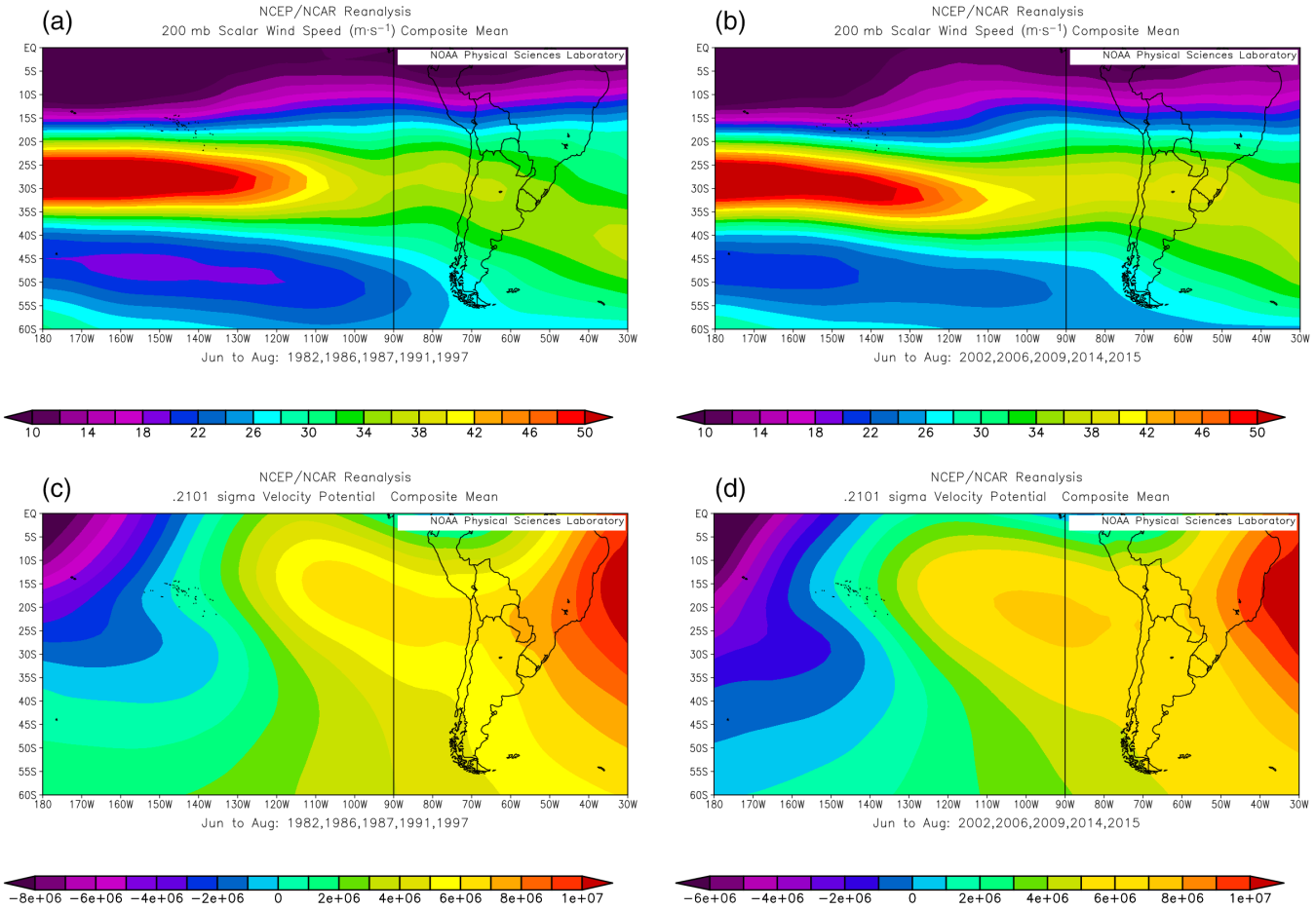

FIGURE 11 Mean composites of (a) and (b) 200-hPa scalar wind speed ($m \cdot s^{-1}$) and (c) and (d) velocity potential at 0.201 sigma level (approximately 200 hPa) for June, July and August during (a) and (c) EN/PDO (+) and (b) and (d) EN/PDO (−). The contour interval in (a) and (b) is 2 $m \cdot s^{-1}$, and for (c) and (d) is 1.0×10^6 $m^2 \cdot s^{-1}$ [Colour figure can be viewed at wileyonlinelibrary.com]

Another issue noticed in this study was related to the variations in the subtropical jet stream. Usually, the jet stream has stronger jet cores during EN compared to LN for DJF and the opposite occurs during JJA, this pattern is maintained during both PDO phases. Certainly, the PDO influences over the jet stream have been shown to be strengthened through all the seasons during PDO (−). This is in agreement with Andreoli and Kayano (2005) who found a strengthened subtropical jet during the negative PDO for DJF as their study was focused on that trimester. Moreover, Figures 11–14 are showing the composite mean per seasons of 200-hPa scalar wind speed and velocity potential at 0.210 sigma level; these composites are comparing EN years during the positive and negative PDO.

A jet core is observed across the Pacific Ocean during JJA with wind speeds around 50 $m \cdot s^{-1}$ dominating the upper-level circulation, noticeably this jet core is displaced eastward in PDO (−) (Figure 11b), the equatorward exit region is located upstream of South America and the associated convergence (positive values of velocity potential) is present in both PDOs with a stronger centre of convergence during PDO (−) (Figure 11d), convergence aloft would favour divergence below which is in agreement with positive anomalies of geopotential height that would have produced the warmer condition in maximum temperature for JJA. This is also consistent with the increased frequency of blocking during these years noted above. For the following fall season, a jet core over northern Argentina/Southern Bolivia appears in addition to the jet core over the Pacific, with higher wind speeds in PDO (−) (Figure 12b). We can observe how the two jet streaks interact as shown by many studies, the equatorward exit part of the Pacific Ocean jet streak and the poleward entrance of the jet streak over South America are both related with convergence producing a centre of maximum convergence over the west coast of South America slightly inclined Northwest- Southeast which is strengthened in PDO (−) (Figure 12d). The characteristics of these jet streaks for the spring season are similar to the fall, with the two jet cores working together to increase the area of convergence upstream of South America (Figure 13). Those trimesters with centres of convergence

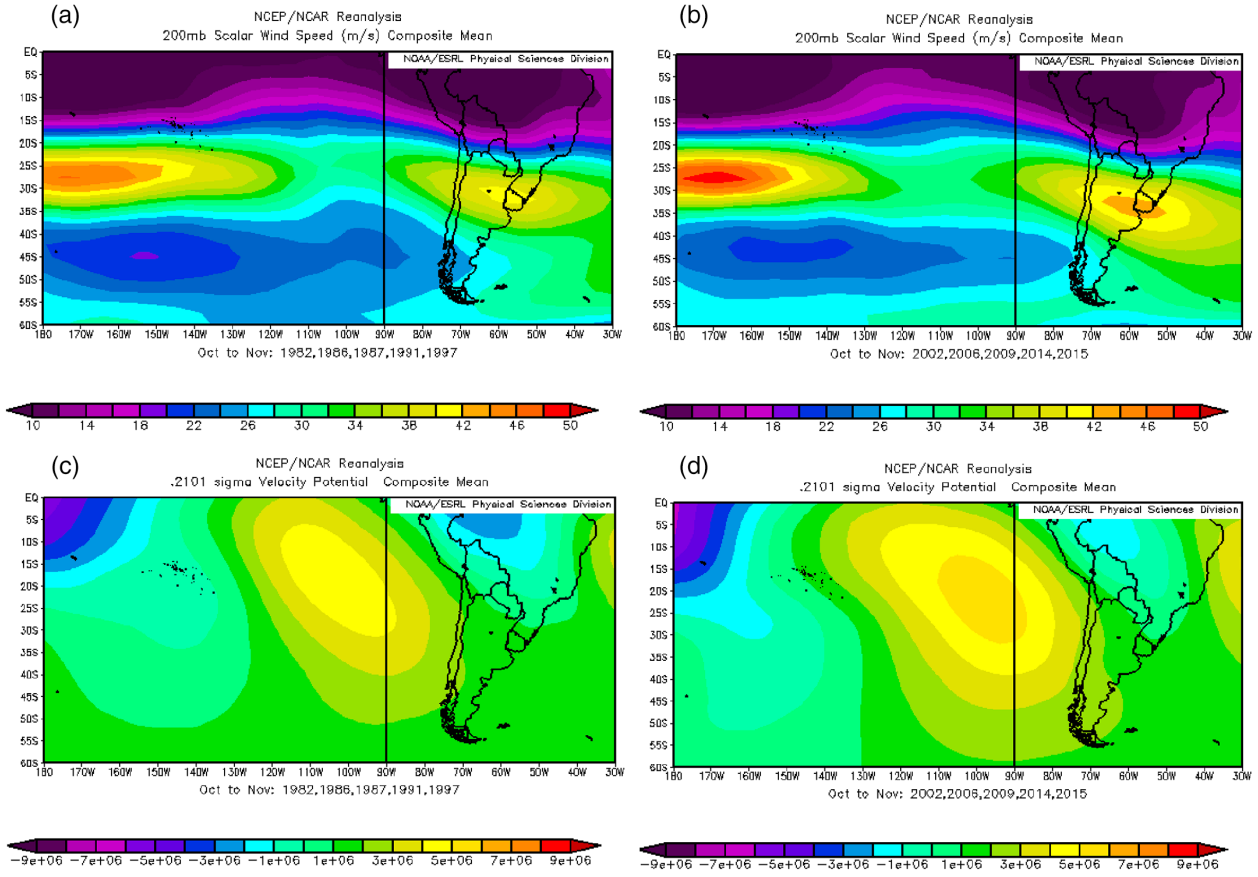

FIGURE 12 As in Figure 11, except for October and November [Colour figure can be viewed at wileyonlinelibrary.com]

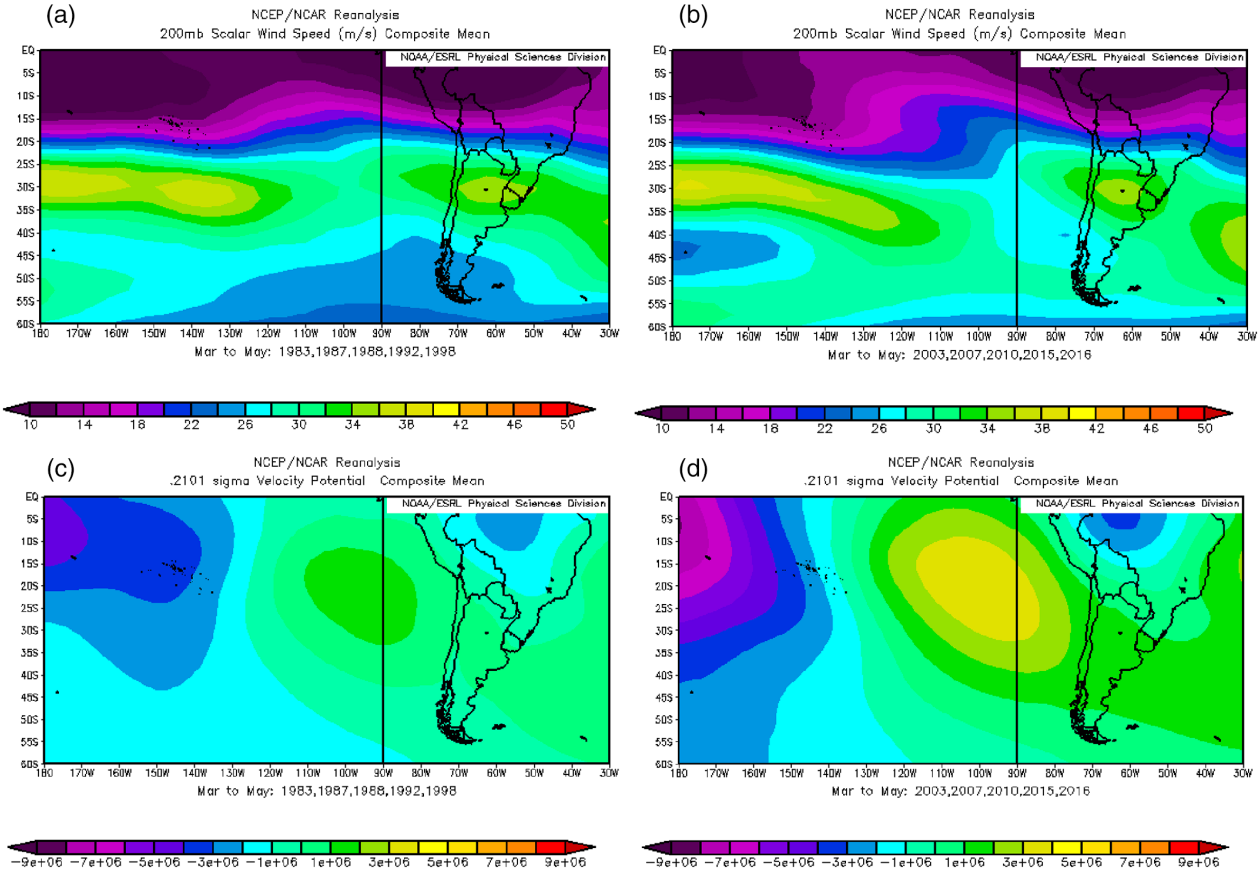

FIGURE 13 As in Figure 11, except for March, April and May [Colour figure can be viewed at wileyonlinelibrary.com]

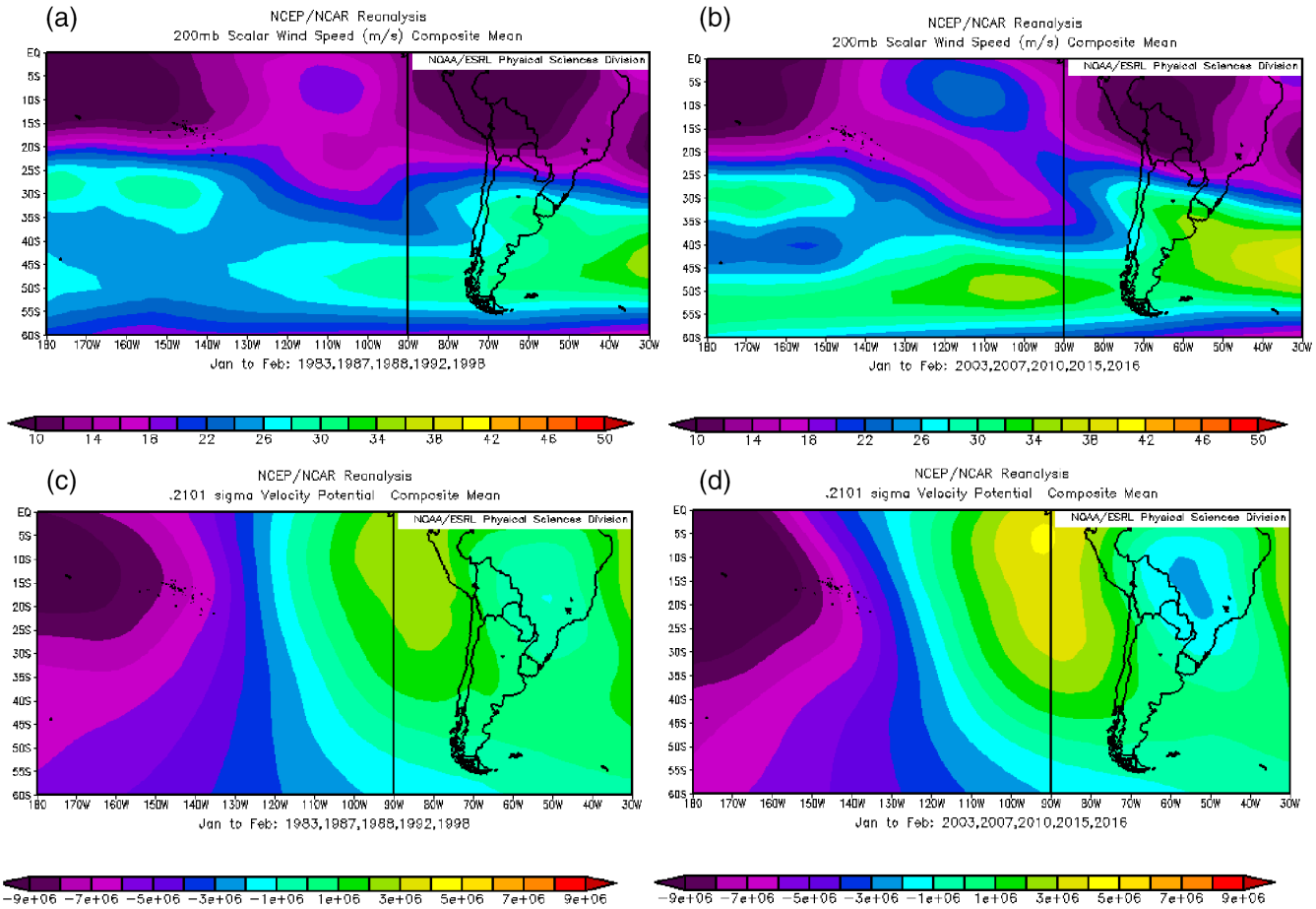

FIGURE 14 As in Figure 11, except for January and February [Colour figure can be viewed at wileyonlinelibrary.com]

near to Bolivia could have influenced the warmer anomalies in maximum temperature as divergence is favoured below, that need to be more explored.

For the winter season (Figure 14), the jet stream is displaced poleward reducing winds speed upstream of South America, although the equatorward entrance of a jet streak is observed downstream South America which is associated with divergence (negative values of velocity potential; Figure 14c,d), these values are strengthened for PDO(−) over Bolivia and Brazil (Figure 14d). Divergence aloft could enhance convergence below which at the same time might be related to the southern position of BH and more wet episodes during EN/PDO (−) compared to PDO (+) for this trimester.

5 | CONCLUSION

The results of this study have shown the PDO influence over ENSO and how these oscillations affect the local climate. The three variables studied have shown an interannual and interdecadal signal in the power spectra analysis along with a strong annual and seasonal cycle. The PDO influence was reflected on EN and NEU phases during DJF as more dry precipitation anomalies were observed during EN/PDO (+) compared to PDO (−), this was associated with a southward displacement of the BH in the current PDO phase, increasing divergence aloft needed to support upward motion over the Bolivian Altiplano. During NEU years, more wet anomalies observed in PDO (+) were in agreement with a weak westerly flow. The ENSO variability is associated with changes in the predominant mid-latitude teleconnection patterns in the southern hemisphere as well as with Pacific Region blocking.

On the other hand, mid-level atmosphere (500-hPa) positive anomalies of geopotential height suggests an increment in the high pressure systems that would possibly increase the maximum temperatures reflected in more warm anomalies and consequently a reduction of cold anomalies for the current PDO(−) phase, especially for JJA, SON and MAM. Previously, the last decade's increment in temperature was mainly attributed to climate change; however, this study is suggesting that PDO could be also partially responsible for that increment, a conclusion strengthened by the influence over the jet

stream and blocking. This is consistent with Zhang and Delworth (2016) which showed that both mechanisms are important and not independent. Additionally, this suggests that the complex ENSO behaviour over the region is quite related to the PDO as well, at least in part. Nonetheless, the results related to PDO need to be verified in future studies with longer time series. A more complicated situation occurs with minimum temperature as warm anomalies of minimum temperature were identified in the current PDO phase, although not all the meteorological stations have the same signal. These results could be impacted by reduced data quality. A more detailed study on cloudiness dynamics and water vapour could help to understand the local variation in minimum temperature anomalies.

The combined PDO and ENSO influence over the Bolivian Altiplano does not fully explain the variability over the region but set upper-level conditions that could favour certain meteorological activity that need to be related with other features such as the BH location and strength, zonal wind anomalies and mid-latitude circulations that are modulated by the jet stream. These results improve the understating on climate variability over the Bolivian Altiplano not only for precipitation, but also for warm and cold anomalies and gives notions for seasonal forecasting based on the influence of ENSO and PDO, which will be the subject of further study.

ACKNOWLEDGEMENTS

The authors want to thank the reviewers for their helpful comments, which have made this work much stronger.

CONFLICT OF INTEREST

The authors declare that there is no conflict of interest regarding the publication of this article.

AUTHOR CONTRIBUTIONS

Katherine Rojas Murillo: Formal analysis; investigation; methodology; software; validation; writing – original draft; writing – review and editing. **Anthony Lupo:** Conceptualization; data curation; investigation; project administration; supervision; writing – review and editing. **Magali Garcia:** Conceptualization; investigation; methodology; supervision; writing – review and editing. **Jere Gilles:** Conceptualization; investigation; project administration; writing – review and editing. **Alex Korner:** Formal analysis; investigation; methodology; validation; writing – original draft. **Marco Rivera:** Formal analysis; validation; writing – review and editing.

ORCID

Katherine Rojas-Murillo https://orcid.org/0000-0001-9614-4815

Anthony R. Lupo https://orcid.org/0000-0002-5810-5652

REFERENCES

Ashok, S., Behera, K., Rao, S.A., Weng, H. and Yamagata, T. (2007) El Niño Modoki and its possible teleconnection. *Journal of Geophysical Research: Oceans*, 112(C11), 1–27. https://doi.org/10.1029/2006JC003798.

Amaya, A.G., Villazon, M.F. and Willems, P. (2018) Assessment of rainfall variability and its relationship to ENSO in a sub-Andean watershed in central Bolivia. *Water (Switzerland)*, 10(6), 1–15. https://doi.org/10.3390/w10060701.

Andrade, M., Lavado-casimiro, W., Brönnimann, S., Moreno, I., Calle, J.M., Ticona, L., Blacutt, L., Lavado-casimiro, W., Sabino, E., Huerta, A., Aybar, C., Hunziker, S., Imfeld, N., Zamuriano, M. (2018) *Climate and Extreme Events from the Central Altiplano of Peru and Bolivia 1981–2010*. Geographica Bernensia. https://doi.org/10.4480/GB2018.N01.

Andreoli, R.V. and Kayano, M.T. (2005) ENSO-related rainfall anomalies in South America and associated circulation features during warm and cold Pacific decadal oscillation regimes. *International Journal of Climatology*, 25(15), 2017–2030. https://doi.org/10.1002/joc.1222.

Birk, K., Lupo, A.R., Guinan, P. and Barbieri, C.E. (2010) The interannual variability of midwestern temperatures and precipitation as related to the ENSO and PDO. *Atmosfera*, 23(2), 95–128.

Bjerknes, J. (1969) Atmospheric teleconnections from the equatorial Pacific. *Monthly Weather Review*, 97(3), 163–172. https://doi.org/10.1175/1520-0493(1969)097<0163:atftep>2.3.co;2.

Bove, M.C., Elsner, J.B., Landsea, C.W., Niu, X. and O'Brien, J.J. (1998) Effect of El Nino on U.S. Landfalling Hurricanes, revisited. *Bulletin of the American Meteorological Society*, 79(11), 2477–2482.

Cai, W., McPhaden, M.J., Grimm, A.M., Rodrigues, R.R., Taschetto, A.S., Garreaud, R.D., Dewitte, B., Poveda, G., Ham, Y-G., Santoso, A., Ng, B., Anderson, W., Wang, G., Geng, T., Jo, H.-S., Marengo, J.A., Alves, L.M., Osman, M., Li, S., Wu, L., Karamperidou, C., Takahashi, K., and Vera, C. (2020) Climate impacts of the El Niño–Southern Oscillation on South America. *Nature Reviews Earth & Environment*, 1(4), 215–231. http://dx.doi.org/10.1038/s43017-020-0040-3

Canedo-Rosso, C., Hochrainer-Stigler, S., Pflug, G., Condori, B. and Berndtsson, R. (2021) Drought impact in the Bolivian Altiplano agriculture associated with the El Niño–Southern Oscillation using satellite imagery data. *Natural Hazards and Earth System Sciences*, 21(3), 955–1010. https://doi.org/10.5194/nhess-21-995-2021

Canedo-Rosso, C., Uvo, C.B. and Berndtsson, R. (2019) Precipitation variability and its relation to climate anomalies in the Bolivian Altiplano. *International Journal of Climatology*, 39(4), 2096–2107. https://doi.org/10.1002/joc.5937.

Canedo Rosso, C., Hochrainer-Stigler, S., Pflug, G., Condori, B. and Berndtsson, R. (2018) Early warning and drought risk assessment for the Bolivian Altiplano agriculture using high resolution satellite imagery data. *Natural Hazards and Earth System Sciences Discussions*, 1–23. https://doi.org/10.5194/nhess-2018-133.

da Silva, G.A.M., Drumond, A. and Ambrizzi, T. (2011) The impact of El Niño on South American summer climate during different

phases of the Pacific Decadal Oscillation. *Theoretical and Applied Climatology*, 106(3–4), 307–319. https://doi.org/10.1007/s00704-011-0427-7.

Gu, D. and Philander, S.G.H. (1995) Secular changes of annual and interannual variability in the tropics during the past century. *Journal of Climate*, 8(4), 864–876.

Folland, C.K., Renwick, J.A., Salinger, M.J. and Mullan, A.B. (2002) Relative influences of the Interdecadal Pacific Oscillation and ENSO on the South Pacific convergence zone. *Geophysical Research Letters*, 29(13), 2–5. https://doi.org/10.1029/2001GL014201.

Garreaud, R.D., Vuille, M., Compagnucci, R. and Marengo, J. (2009) Present-day South American climate. *Palaeogeography, Palaeoclimatology, Palaeoecology*, 281(3–4), 180–195. https://doi.org/10.1016/j.palaeo.2007.10.032.

Garreaud, R. and Aceituno, P. (2001) Interannual rainfall variability over the South American Altiplano. *Journal of Climate*, 14(12), 2779–2789. https://doi.org/10.1175/1520-0442(2001)014<2779:IRVOTS>2.0.CO;2.

Garreaud, R., Vuille, M. and Clement, A.C. (2003) The climate of the Altiplano: observed current conditions and mechanisms of past changes. *Palaeogeography, Palaeoclimatology, Palaeoecology*, 194(1–3), 5–22. https://doi.org/10.1016/S0031-0182(03)00269-4.

Gershunov, A. and Barnett, T.P. (1998) Interdecadal modulation of ENSO teleconnections. *Bulletin of the American Meteorological Society*, 79(12), 2715–2725.

Goodrich, G.B. and Goodrich, G. (2004) Arizona-Nevada academy of science modulation of the winter ENSO Arizona climate signal by the Pacific decadal oscillation modulation of the winter ENSO Arizona climate signal by the Pacific Decadal Oscillation. *Journal of the Arizona-Nevada Academy of Science*, 36(2), 88–94.

Henson, C., Market, P., Lupo, A. and Guinan, P. (2017) ENSO and PDO-related climate variability impacts on Midwestern United States crop yields. *International Journal of Biometeorology*, 61(5), 857–867. https://doi.org/10.1007/s00484-016-1263-3.

Hunziker, S., Brönnimann, S., Calle, J., Moreno, I., Andrade, M., Ticona, L., Huerta, A. and Lavado-Casimiro, W. (2018) Effects of undetected data quality issues on climatological analyses. *Climate of the Past*, 14(1), 1–20. https://doi.org/10.5194/cp-14-1-2018.

Hunziker, S., Gubler, S., Calle, J., Moreno, I., Andrade, M., Velarde, F., Ticona, L., Carrasco, G., Castellón, Y., Oria, C., Croci-Maspoli, M., Konzelmann, T., Rohrer, M. and Brönnimann, S. (2017) Identifying, attributing, and overcoming common data quality issues of manned station observations. *International Journal of Climatology*, 37(11), 4131–4145. https://doi.org/10.1002/joc.5037.

IRI. (2019). IRI/LDEO Climate Data Library. Climatologies and Standardized Anomalies. http://iridl.ldeo.columbia.edu/dochelp/StatTutorial/Climatologies/index.html

Kalnay, E., Kanamitsu, M., Kistler, R., Collins, W., Deaven, D., Gandin, L., Iredell, I., Saha, S., White, G., Woollen, J., Zhu, Y., Chelliah, M., Ebisuzaki, W., Higgins, W., Janowiak, J., Mo, K.C., Ropelewski, C., Wang, J., Leetma, A., Reynolds, R., Jenne, R. and Joseph, D. (1996) The NCEP/NCAR 40-year reanalysis project. *The Bulletin of the American Meteorological Society*, 77, 437–471.

Kayano, M.T. and Andreoli, R.V. (2009) Relations of the South American summer rainfall interannual variations with the Pacific Decadal Oscillation. *International Journal of Climatology*, 29(3), 317–319. https://doi.org/10.1002/joc.

Kistler, R., Kalnay, E. and Collins, W. (2001) The NCEP-NCAR 50-year reanalysis: monthly means CD-ROM and documentation. *The Bulletin of the American Meteorological Society*, 82, 247–267.

Krishnamurti, T., Stefanova, L. and Misra, V. (2013) *Tropical Meteorology—An Introduction*, 2013th edition. New York, NY: Springer. https://doi.org/10.1007/978-1-4614-7409-8.

Kung, E.C. and Chern, J.G. (1995) Prevailing anomaly patterns of the Global Sea surface temperatures and tropospheric responses. *Atmósfera*, 8, 99–114.

Lupo, A., Jensen, A., Mokhov, I., Timazhev, A., Eichler, T. and Efe, B. (2019) Changes in global blocking character in recent decades. *Atmosphere*, 10(2), 92. https://doi.org/10.3390/atmos10020092.

Lupo, A., Kelsey, E.P., Weitlich, D.K., Davis, N.A. and Market, P.S. (2008) Using the monthly classification of global SSTS and 500 hPa height anomalies to predict temperature and precipitation regimes one to two seasons in advance for the mid-Mississippi region. *National Weather Association Digest*, 32(1), 23.

Lupo, A.R., Kelsey, E.P., Weitlich, D.K., Woolard, J.E., Mokhov, I. I., Guinan, P.E. and Akyüz, F.A. (2007) Interannual and interdecadal variability in the predominant Pacific region SST anomaly patterns and their impact on climate in the mid-Mississippi valley region. *Atmosfera*, 20(2), 171–196.

Lupo, A.R., Hayward, R.S. and Whitledge, G.W. (2012) Synchronization of fishes' temporal feeding patterns with weather in mid-Missouri. *Journal of Freshwater Ecology*, 2012, 37–41. https://doi.org/10.1080/02705060.2012.666927.

Mantua, N.J., Hare, S.R., Zhang, Y., Wallace, J.M. and Francis, R.C. (1997) A Pacific decadal climate oscillation with impacts on salmon. *Bulletin of the American Meteorological Society*, 78, 1069–1079. https://doi.org/10.1175/1520-0477(1997)078%3C1069:APICOW%3E2.0.CO%5Cn2.

Mantua, N.J. and Hare, S.R. (2002) The pacific decadal oscillation. *Journal of Oceanography*, 58, 35–44.

Mokhov, I.I., Khvorostyanov, D.V. and Eliseev, A.V. (2004) Decadal and longer term changes in El Niño – Southern oscillation characteristics. *International Journal of Climatology*, 24(4), 401–414. https://doi.org/10.1002/joc.1013.

Newman, M., Alexander, M.A., Ault, T.R., Cobb, K.M., Deser, C., Di Lorenzo, E., Mantua, N.J., Miller, A.J., Minobe, S., Nakamura, H., Schneider, N., Vimont, D.J., Phillips, A.S., Scott, J.D. and Smith, C.A. (2016) The Pacific decadal oscillation, revisited. *Journal of Climate*, 29(12), 4399–4427. https://doi.org/10.1175/JCLI-D-15-0508.1.

O'Kane, T.J., Monselesan, D.P. and Risbey, J.S. (2017) A multiscale reexamination of the Pacific–South American pattern. *Monthly Weather Review*, 145, 379–402.

Oliveira, F.N.M., Carvalhoc, L.M.V. and Ambrizzi, T. (2014) A new climatology for southern hemisphere blockings in the winter and the combined effect of ENSO and SAM phases. *International Journal of Climatology*, 34, 1676–1692.

Perry, L.B., Seimon, A., Andrade-Flores, M.F., Endries, J.L., Yuter, S. E., Velarde, F., Arias, S., Bonshoms, M., Burton, E.J., Winkelmann, I.R., Cooper, C.M., Mamani, G., Rado, M., Montoya, N. and Quispe, N. (2017) Characteristics of precipitating storms in glacierized tropical Andean cordilleras of Peru and Bolivia. *Annals of the American Association of Geographers*, 107(2), 309–322. https://doi.org/10.1080/24694452.2016.1260439.

Ren, H., Jin, F-F. (2013) Recharge oscillator mechanisms in two types of ENSO. *J. climate*, 26(17), 6506–6523.

Segura, H., Espinoza, J.C., Jungquas, C., Lebel, T., Vuille, M. and Garreaud, R. (2020) Recent changes in precipitation-driving processes over the southern tropical Andes/western Amazon. *Climate Dynamics*, 54, 2613–2631. https://doi.org/10.1007/s00382-020-05132-6.

Segura, H., Junquas, C., Espinoza, J.C., Vuille, M., Jauregui, Y.R., Rabatel, A., Condom, T. and Lebel, T. (2019) New insights into the rainfall variability in the tropical Andes on seasonal and interannual time scales. *Climate Dynamics*, 53(1–2), 405–426. https://doi.org/10.1007/s00382-018-4590-8.

Segura, H., Espinoza, J.C., Clementine, J. and Takahashi, K. (2016) Evidencing decadal and interdecadal hydroclimatic variability over the Central Andes. *Environmental Research Letters*, 11(9), 094016. https://doi.org/10.1088/1748-9326/11/9/094016

Seiler, C., Hutjes, R. and Kabat, P. (2013) Climate variability and trends in Bolivia. *Journal of Applied Meteorology and Climatology*, 52, 130–146. https://doi.org/10.1175/JAMC-D-12-0105.1.

Shapiro, R. (1970) Smoothing, filtering, and boundary effects. *Reviews of Geophysics*, 8(2), 737–761. https://doi.org/10.1029/RG008i002p00359.

Stueker, M.F. (2018) Revisiting the Pacific meridional mode. *Scientific Reports*, 8, 3216. https://doi.org/10.1038/s41509-018-21537-0.

Takahashi, K., Montecinos, A., Goubanova, K. and Dewitte B. (2011) ENSO regimes: Reinterpreting the canonical and Modoki El Niño. *Geophysical Research Letters*, 38(10), L10704. http://dx.doi.org/10.1029/2011gl047364

Tilly, D.E., Lupo, A.R., Melick, C.J. and Market, P.S. (2008) Calculated height tendencies in a Southern Hemisphere blocking and cyclone event: the contribution of diabatic heating to block intensification. *Monthly Weather Review*, 136, 3568–3578. http://doi.org/10.1029/2011gl047364

Vuille, M., Bradley, R.S. and Keimig, F. (2000) Interannual climate variability in the Central Andes and its relation to tropical Pacific and Atlantic forcing. *Journal of Geophysical Research*, 105(10), 12447–12460. https://doi.org/10.1175/1520-0442(2000)013<2520:CVITAO>2.0.CO;2.

Vuille, M. and Keimig, F. (2004) Interannual variability of summertime convective cloudiness and precipitation in the central Andes derived from ISCCP-B3 data. *Journal of Climate*, 17(17), 3334–3348. https://doi.org/10.1175/1520-0442(2004)017<3334:IVOSCC>2.0.CO;2.

Wang, H., Kumar, A., Wang, W. and Xue, Y. (2012) Influence of ENSO on Pacific decadal variability: an analysis based on the NCEP climate forecast system. *Journal of Climate*, 25, 6136–6151.

Wang, H. and Fu, R. (2004) Influence of cross-Andes flow on the South American low-level jet. *Journal of Climate*, 17, 1247–1262.

Wilks, D.S. (2006) Statistical methods in the atmospheric sciences. In: *International Geophysics Series* (p. 627). Cambridge, MA: Academic Press. https://doi.org/10.1002/met.16.

Zhang, L. and Delworth, T.L. (2016) Simulated response of the Pacific Decadal Oscillation to climate change. *Journal of Climate*, 29(16), 5999–6018.

How to cite this article: Rojas-Murillo, K., Lupo, A. R., Garcia, M., Gilles, J., Korner, A., & Rivera, M. A. (2021). ENSO and PDO related interannual variability in the north and east-central part of the Bolivian Altiplano in South America. *International Journal of Climatology*, 1–27. https://doi.org/10.1002/joc.7374

APPENDIX A

ANOVA results of the effect of PDO and ENSO phases on monthly precipitation, maximum and minimum temperatures

Tables A1 and A2

TABLE A1 The seasonal precipitation (mm) for the stations in the study region as partitioned by ENSO and PDO phase

Station	Spring	Summer	Fall	Winter
Achiri				
Overall	57.1	299.4	97.5	14.8
EN	54.9	**238.1***	101.6	12.3
LN	**27.6**	301.2	85.8	**0.8***
NEU	64.1	**326.1**	98.1	18.8
PDO+	**76.7****	293.0	104.5	**17.1**
PDO−	**35.3****	306.9	90.2	**12.5**
Ayo Ayo				
Overall	78.0	219.6	74.5	19.3
EN	84.3	193.1	78.5	20.8
LN	60.2	191.2	79.2	**8.8**
NEU	78.8	236.9	71.8	20.8
PDO+	86.9	233.0	85.5	19.6
PDO−	68.2	204.1	62.93	19.0
Calacoto				
Overall	51.7	273.3	83.7	12.0
EN	47.3	228.5	81.7	8.1
LN	40.6	239.0	98.4	5.0
NEU	56.0	299.8	81.7	15.2
PDO+	57.4	262.5	76.7	**14.1**
PDO−	45.4	285.8	91.1	**9.9**
Copacabana				
Overall	135.7	432.0	195.3	36.9
EN	135.3	**362.3**	201.1	37.0
LN	**93.7**	438.8	**150.7**	25.4
NEU	144.6.0	461.3	201.7	39.2
PDO+	148.9	392.2	181.0	**41.8**
PDO−	121.0	478.0	210.2	**31.8**
EL Alto				
Overall	126.7	330.9	131.7	27.3
EN	128.6	**303.4**	134.2	25.6
LN	**83.4***	297.5	110.0	19.3
NEU	134.8	**349.7**	134.9	29.6
PDO+	133.8	317.7	136.0	30.1
PDO−	118.8	346.3	127.1	24.3

(Continues)

TABLE A1 (Continued)

Station	Spring	Summer	Fall	Winter
EL Belen				
Overall	86.1	235.8	89.4	29.6
EN	73.2	221.5	90.1	25.8
LN	75.0	233.8	80.4	27.3
NEU	94.3	242.5	90.8	31.6
PDO+	91.1	242.1	98.0	32.6
PDO−	80.5	228.5	80.3	26.3
Oruro				
Overall	77.6	251.1	85.2	19.6
EN	80.5	**210.0**	78.7	21.9
LN	**55.8**	204.9	102.1	12.1
NEU	80.8	**278.4**	84.7	20.1
PDO+	78.9	231.6	84.3	17.9
PDO−	76.2	273.6	86.1	21.4
Patacamaya				
Overall	76.2	237.1	74.6	17.0
EN	74.9	223.9	84.4	18.9
LN	**47.0***	**198.1**	72.6	8.7
NEU	82.8	250.7	70.7	17.9
PDO+	**87.6**	236.3	79.5	17.1
PDO−	**63.5**	238.1	69.5	17.0
Tiawanacu				
Overall	99.7	284.3	110.0	23.0
EN	93.2	**241.6***	111.7	22.5
LN	77.4	**204.2***	**61.9***	13.5
NEU	107.3	**319.1***	118.8	25.1
PDO+	**124.7****	310.8	**130.4***	**26.1**
PDO−	**72.1****	253.5	**88.5***	**19.7**

Note: Bold values (*,**) indicate a statistically significant difference from the overall mean at $p = .10$ ($p = .05$, $p = .01$).

TABLE A2 As in Table A1, except for the maximum and minimum seasonal temperature (°C) information

Station	Spring	Summer	Fall	Winter
Ayo Ayo				
Overall	17.9/−1.5	17.5/3.4	17.6/−2.2	16.5/−9.5
EN	17.1/−1.9	**18.4***/3.7	**18.2**/−2.1	17.1/−9.4
LN	18.9/**−2.4***	17.9/3.4	17.6/−2.0	17.2/−9.5
NEU	18.1/**−1.1***	**17.1***/3.4	17.3/−2.2	**16.2**/−9.5
PDO+	**17.4*/−0.9****	**16.8**/3.7****	**16.7**/−1.7****	**15.6**/−9.1****
PDO−	**18.5**/−2.1****	**18.4**/3.0****	**18.6**/−2.7****	**17.6**/−10.0****
Calacoto				
Overall	19.4/−3.1	18.8/2.6	18.1/−2.4	16.6/−9.7
EN	18.5/−3.4	**19.8****/2.4	**18.8****/−2.4	**17.2***/−9.7

TABLE A2 (Continued)

Station	Spring	Summer	Fall	Winter
LN	20.0/**−4.0***	18.7/2.6	17.7/−2.6	16.6/−9.8
NEU	19.6/**−2.7***	**18.4***/2.6	17.9/−2.4	**16.3**/−9.7
PDO+	19.2/**−2.6****	**18.6****/2.6	**17.7****/**−2.3**	**16.1****/**−9.4****
PDO−	19.6/**−3.6****	**19.2****/2.5	**18.6****/**−2.6**	**17.1****/10.1****
EL Alto				
Overall	15.3/1.0	14.6/3.7	14.5/0.9	13.9/−3.5
EN	14.6/0.9	**15.4****/3.9	**15.2****/1.1**	**14.4***/−3.3
LN	16.0/**0.4****	14.6/3.6	14.3/0.6	**13.4**/−3.9
NEU	15.5/**1.2***	**14.2***/3.6	**14.3**/0.8	13.8/−3.5
PDO+	15.2/**1.1***	14.5/**3.4****	**14.3****/1.0*	**13.6****/**−3.1****
PDO−	15.4/**0.9***	14.7/**4.0****	**14.8****/0.7*	**14.2****/**−3.9****
EL Belen				
Overall	15.5/0.2	15.1/3.3	15.2/−0.6	14.1/−5.7
EN	15.1/**−0.3***	**15.7****/3.3	**15.5***/**−0.2**	**14.6***/−5.6
LN	15.6/0.1	**14.6**/3.2	**14.6***/−0.7	14.0/−5.5
NEU	15.7/**0.4**	15.0/3.2	15.1/−0.7	13.9/−5.7
PDO+	15.6/**0.3**	15.2/3.2	15.1/**−0.4***	**13.8****/**−5.4***
PDO−	15.4/**0.0**	15.0/3.3	15.2/**−0.8***	**14.4****/**−5.9***
Oruro				
Overall	19.2/0.4	19.1/5.0	18.3/0.1	16.1/−7.2
EN	18.2/0.0	**20.0****/4.8	**18.9***/0.1	**16.7***/−7.0
LN	20.1/**−0.4**	19.5/5.2	18.4/0.0	16.3/−7.4
NEU	19.5/**0.7**	**18.6***/5.0	**18.0**/0.1	15.8/−7.3
PDO+	**18.8/0.1***	**18.5****/4.4****	**17.6****/**−0.4****	**15.3****/**−7.7****
PDO−	**19.7/0.6***	**19.7****/5.6****	**19.1****/0.6****	**16.9****/**−6.7****
Patacamaya				
Overall	18.5/1.2	18.2/4.6	18.3/0.4	17.0/−5.0
EN	17.7/0.9	**19.0***/4.8	**18.8***/**0.9***	**17.4**/**−4.1***
LN	18.8/1.0	17.8/4.8	17.8/0.5	16.7/−5.1
NEU	18.9/1.3	18.0/4.5	18.1/**0.1**	16.8/−5.4
PDO+	18.7/**0.7****	18.2/**4.2****	**17.9****/0.1*	**16.4****/**−5.6****
PDO−	18.4/**1.7****	18.3/**5.1****	**18.7****/0.6*	**17.5****/**−4.4****
Tiawanacu				
Overall	17.3/0.1	16.7/3.7	16.5/−0.3	15.4/−6.3
EN	16.4/−0.1	**17.3****/3.9	**16.8**/0.0	**16.0****/−6.5
LN	17.8/**−0.9***	16.5/3.6	16.1/−0.4	15.1/−6.1
NEU	17.6/**0.4**	**16.5**/3.7	16.4/−0.4	**15.2**/−6.2
PDO+	17.5/**−0.12****	16.8/**3.5****	**16.3***/−0.3	15.3/**−6.6***
PDO−	17.1/**0.4****	16.6/**4.0****	**16.6***/−0.3	15.5/**−5.9***